ACS OMEGA

http://pubs.acs.org/journal/acsodf

Article

Iron Sulfide Scale Inhibition in Carbonate Reservoirs

Nijat Gasimli, Mohamed Mahmoud,* Muhammad Shahzad Kamal,* Shirish Patil, Hamad A. Alsaiari, and Ibnelwaleed A. Hussein

Cite This: *ACS Omega* 2022, 7, 26137−26153

Read Online

ACCESS | Metrics & More | Article Recommendations

ABSTRACT: Hydrocarbon production operations include water injection, varying stimulation approaches, and enhanced oil recovery techniques. These treatments often affect reservoir formation, production, and injection facilities. Such sorts of well operations cause the formation of organic and inorganic scales in the near-wellbore region and various production and injection structures. Downhole squeeze treatment is commonly used as a control measure to prevent scale precipitation. A scale inhibitor solution is introduced into a formation by applying a squeeze treatment. The method allows scale inhibitors to adsorb on the internal rock surface to avoid settling down the scale precipitates. Thus, the study of adsorption of different types of inhibitors to prevent scale formation on the reservoir rock through the execution of downhole squeeze treatment is becoming necessary. This study incorporated different experimental techniques, including dynamic adsorption experiments of chelating agents employing a coreflooding setup, inductively coupled plasma-optical emission spectrometry (ICP-OES) to inhibit the formation of iron-containing scales in limestone rocks, and ζ-potential measurements targeting determination of iron precipitation in varying pH environments on calcite minerals. The influence of the inhibitor soaking time and salt existence in the system on chelating agent adsorption was also evaluated in the coreflooding experiments. The findings based on the coreflooding tests reveal that the concentration of chelating agents plays a significant role in their adsorption on carbonate rocks. The treatments with 20 wt % ethylenediaminetetraacetic acid (EDTA) and 20 wt % diethylenetriaminepentaacetic acid produced the highest adsorption capacity in limestone rock samples by inhibiting 84 and 85% of iron(III) ions, respectively. Moreover, the presence of the salts ($CaCl_2$ and $MgCl_2$) considerably decreased the adsorption of 10 wt % EDTA to 56% ($CaCl_2$) and 52% ($MgCl_2$) and caused nearly 20% more permeability reduction, while more inhibitor soaking time resulted in comparably higher adsorption and lesser permeability diminution. The results of ζ-potential measurements showed that the pH environment controls iron(II) and (III) precipitation, and iron(III) starts to deposit from a low pH region, whereas iron(II) precipitates in increased pH environments in calcite minerals.

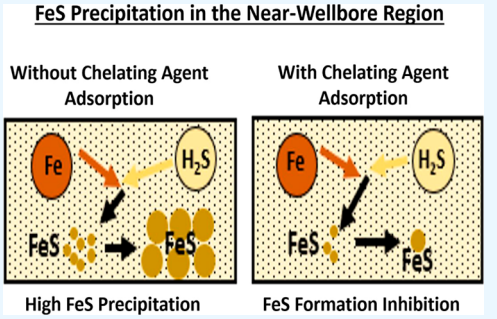

INTRODUCTION

Positively charged ions precipitate and react with various negatively charged ions in a wide variety of oilfield production and injection operations resulting in the formation of inorganic scales. Scale deposits significantly limit the productivity of oil and gas production wells and the full injectivity potential of injection wells by blocking the inner diameter of tubing strings, accumulating on the surface and downhole equipment and reducing permeability of the near-wellbore regions.[1−3] Scale control is accomplished either by removing the existing scale precipitates or inhibiting the formation of varying scale deposits. The chemistry, performance, metal complexing mechanisms of metal control chemicals (inhibitors), and mitigation methods of inorganic scales were previously studied.[4−8] Chelating agents are a class of these chemicals used in the upstream oil and gas industry.

Organic compounds with two or more groups (ligands) that can donate electrons to capture or adsorb the positively charged ions (metal ions) are named chelating agents. A variety of chelating agents are utilized within the petroleum industry and in diverse engineering and manufacturing fields.[5,9] Their application in the petroleum industry mainly involves acidizing, hydraulic fracturing, prevention of scale formation, scale removal, filter cake removal, and enhanced oil recovery (EOR).[10−13] Inorganic acids are occasionally employed for stimulation and scale removal. Many other factors contribute to their utility, such as hydrogen sulfide (H_2S) and corrosion, resulting in higher operating costs. Chelating agents have gained attention as an environmentally friendly and cost-effective alternative to conventional chemicals in the last few decades.[9]

Received: March 16, 2022
Accepted: July 11, 2022
Published: July 21, 2022

The two major types of chelating agents are amino-polycarboxylic acids (APCAs) and phosphonates. Diethylene-triaminepentamethylene phosphonic acid, nitriletrimethylene-phosphonic acid, and 1-hydroxyethane-1,1-diphosphonic acid are examples of phosphonates with an extensive range of applications. Many types of APCA chelating agents are used in the oil industry, but ethylenediaminetetraacetic acid (EDTA), diethylenetriaminepentaacetic acid (DTPA), L-glutamic acid-*N*,*N*-diacetic acid (GLDA), and hydroxylethyliminodiacetic acid are the most widely used.[9] However, every chelating agent possesses its unique properties for capturing metals and forming complexes with them in a solution that is quite vital in preventing scale formation, and the property determines the ability of different metals and chelating agents to react and form stable complexes.[14] The stability constants of iron(II) and iron(III) are particularly important to consider when it comes to the formation of iron-containing scales. Among EDTA, DTPA, and GLDA, DTPA and EDTA possess the highest stability constant toward iron(II) and iron(III), while GLDA has the lowest. The optimum pH range for EDTA for capturing Fe(III) and forming a stable complex is from 1 to 11 and from 2 to 11, respectively, for DTPA.[9]

Squeezing treatment or continuous injection is the most common way to inject scale inhibitors into the formation in field applications.[15,16] The squeeze inhibitor technique is considered a successful choice in carbonate rocks.[17] Scale inhibitors work by either altering morphology of the growing sites and adsorption effects.[16] The adsorption effect is explained by the fact that scale-inhibiting molecules bind to the areas where scale-generating molecules should be settled down.[16] The underlying theory behind adsorption effects is that those scale inhibitors retain in the sites where scale generating molecules should deposit. The result would be a lack of growth in scale crystals and an inability to adsorb onto the internal rock surface. The second type of mechanism involves controlling the morphology of the crystal surface by adsorbing inhibitors onto it and hindering the growth of the scale crystals. High pressure (HP), high temperature, and formation water pH play an essential role during scale formation.[18] The most common laboratory techniques for analyzing the effectiveness, growth inhibition, and dispersion mechanisms of inhibitors include static bottle tests, dynamic filter/tube-blocking tests, static adsorption tests, and dynamic adsorption tests—coreflooding.[19,20]

Static bottle tests are used for screening the different types of inhibitors.[21,22] However, some recent literature shows that such laboratory experiments underestimate the amount of scale that can potentially form in dynamic testing methods.[23] The dynamic tube-blocking tests work on tube blockage; they are often used to determine minimum inhibitor concentration. On the other hand, dynamic filter-blocking tests incorporate small-size filters to evaluate the adsorption of scale inhibitors. Static adsorption tests can be utilized to determine the adsorption nature of the scale inhibitor on crushed rock samples. The final technique is dynamic adsorption tests using coreflooding. The method has crucial advantages, such as considering formation damage (permeability changes) and the fact that the system can be designed according to the reservoir conditions to create a more realistic reservoir model.

The adsorption of phosphonates was studied on different formation rocks, including sandstone, calcite, and barite.[17,24,25] The results revealed that the Ca-phosphonate solution complex with neutral pH is adsorbed on the mineral surface at low concentrations. At the same time, it was determined that 7% of the calcite surface was filled with phosphonates at saturation. The adsorption and precipitation tendency of phosphonates, polymer-based, and sulphonated copolymer inhibitors on chalk and limestone rock samples were studied by Jordan and Sjursaether.[26] Sulfonated copolymers showed the mechanism of inhibitor adsorption/desorption, while phosphonate-based inhibitors resulted in a precipitation/dissolution mechanism. A static bottle test setup was used by Bhandari et al.[22] to control the formation of metal sulfide scales utilizing polymeric inhibitors with amide functional groups. The authors claimed that the inhibition mechanism was crystal growth rather than dispersion. The ability of EDTA to adsorb heavy metals, such as arsenic and lead, was studied by Sulastri et al.[27] The study incorporates the Langmuir isotherm model, and adsorption was determined by changing the metal concentration from low to high. EDTA demonstrated a substantial adsorption capacity against As and Pb. In addition to the adsorption studies conducted for scale inhibition, many attempts have been made for quantification and modeling of the adsorption/desorption behavior of the hydrocarbons in shale formations for estimation of shale gas-in-place. Kong et al.[28] studied the adsorption and desorption isotherms of the methane and ethane gas on two different shale samples. Excess adsorption/desorption isotherms of methane and ethane were studied using the thermogravimetric method coupled with the simplified local density theory/Peng−Robinson equation of state (SLD-PR EOS) model for predicting gas adsorption on shale rocks. The model's main advantage is reported as an accurate calculation of adsorption by considering fluid−fluid and fluid−solid interactions. Their work revealed that ethane produces more adsorption capacity compared to methane gas, and the use of the proposed model showed matching results with the experimental data. The absolute adsorption of methane gas on shale was also studied by Liu et al.[29] using the thermogravimetric method and the SLD theory. The theory can take the fluid/pore−surface interactions into account, and the density of adsorbed methane was calculated. The proposed methodology has the ability to predict the absolute gas adsorption as precisely as molecular simulations with a reduced computational cost. The authors claimed that the density distributions of methane gas are significantly affected by the temperature, pressure, and pore size.

The literature contains numerous studies on the adsorption of different types of inhibitors on formation rocks and their inhibition mechanism. However, for the first time, this study is testing the ability of chelating agents to inhibit scale formation. Adsorption of chelating agents in limestone rocks was determined by the power of chelating agents to capture iron ions. The effluent samples containing ferric ions were collected during the experiments. The more iron ions inhibited by chelating agents indicate a higher degree of adsorption on rocks.

To sum up, this research work aims (1) to study the adsorption of aminocarboxylic acids (other than polymeric inhibitors and phosphonates) on carbonate rocks in an attempt to prevent the formation of iron-containing inorganic scales, (2) evaluate the influences of inhibitor concentration, soaking time, and cations on adsorption, (3) identify the pH environments that might induce precipitation of iron(II) and iron(III) crystals in calcite mineral, and (4) analyze the effects of salt type on the precipitation of iron(III) on calcite mineral.

https://doi.org/10.1021/acsomega.2c01568
ACS Omega 2022, 7, 26137−26153

MATERIALS AND METHODS

Materials. *Coreflooding Experiments.* The adsorption of high-pH (pH ∼11) APCA (EDTA, DTPA) on Indiana limestone (IL) rock samples with a length of 6 in. and a diameter of 1.5 in. was studied at an ambient temperature condition [25 °C (77 °F)]. Rock samples were initially saturated with 3 wt % potassium chloride (KCl). Then, a coreflooding system was employed to perform adsorption experiments using 10 IL core samples.

Table 1 represents the chemicals, concentrations, and pH used in the study. Three different concentrations of EDTA (10, 15 wt, and 20 wt %) and one concentration of DTPA (20 wt %) were prepared with a pH of around 11. 20 wt % DTPA was obtained from the dilution of 38 wt % of the DTPA solution, and a high pH was achieved using sodium hydroxide (NaOH) from Sigma-Aldrich. Ferric chloride ($FeCl_3$) solution was prepared with an approximate calculated Fe^{3+} concentration of 3000 ppm. A solution containing 10 wt % EDTA supplemented with 5000 ppm of $MgCl_2$ and $CaCl_2$ was used to study the effect of salts on EDTA adsorption.

Table 1. Chemical Solutions Used in Coreflooding Experiments with Respective Concentrations and pH Values

chemical solutions	concentrations	pH
EDTA	10 wt %	10.80
	15 wt %	11.00
	20 wt %	11.20
EDTA + ($MgCl_2$)	10 wt % + (5000 ppm)	10.90
EDTA + ($CaCl_2$)	10 wt % + (5000 ppm)	11.00
DTPA	20 wt %	11.20
KCl	3 wt %	
$FeCl_3$	∼10,000 ppm (∼3000 ppm Fe^{3+})	3.10

Table 2. Sample Mineral Properties[30]

mineral	chemical formula	molecular weight (g)	density (g/cm^3)
calcite	$CaCO_3$	100.09	2.71
quartz	SiO_2	60.08	2.62

Table 3. Properties of Rock Samples

core no.	PV, cm^3	porosity, %	initial permeability, mD
IL-1	24.2	13.9	19.9
IL-2	23.8	13.7	22.8
IL-3	23.5	13.5	17.9
IL-4	23.9	13.7	17.8
IL-5	22.5	13.0	11.1
IL-6	23.0	13.1	11.0
IL-7	29.5	17.0	17.5
IL-8	24.7	14.2	12.1
IL-9	26.5	14.9	12.5
IL-10	33.1	19.2	49.7

ζ-Potential Measurements. The chemical formulas, molecular weights, and densities of material samples used in ζ-potential measurements are shown in Table 2. Reported mineral densities have an uncertainty of ±0.1%. The calcite mineral sample was crushed to the mean particle size of 4.42 μm. Iron precipitation in calcite minerals was studied at a pH environment ranging from 1 to 13. A buffer solution was prepared, and further pH control was achieved using 0.1 M of nitric acid and sodium hydroxide. Various concentrations of $FeCl_2$ and $FeCl_3$ varying between 100 and 10,000 ppm of Fe^{2+} and Fe^{3+} concentration were prepared as an iron source (Fe^{2+} and Fe^{3+}). The potential effect of sodium chloride (NaCl), magnesium chloride ($MgCl_2$), and calcium chloride ($CaCl_2$) on iron precipitation was further identified.

Core and Sample Preparations. Before coreflooding experiments, core preparation (core cleaning, core cutting), core sample weighting, fluid preparation, and core sample saturation were performed, and core pore volume (PV) and core porosity were determined. The rock core samples were first cleaned with ethanol using a Soxhlet extractor. The cores were then dried in an oven at 70 °C (158 °F). The dry weight of rock samples (M_{dry}) was measured. Furthermore, core samples were exposed to a vacuum pressure for 3−4 h and then were saturated with brine solution (3 wt % KCl) at a pressure of 2000 psi. Brine saturation was performed for 24 h, and the wet weight of the samples (M_{wet}) was measured. The brine density (density of 3 wt % KCl = 1.0175 g/cm^3) and

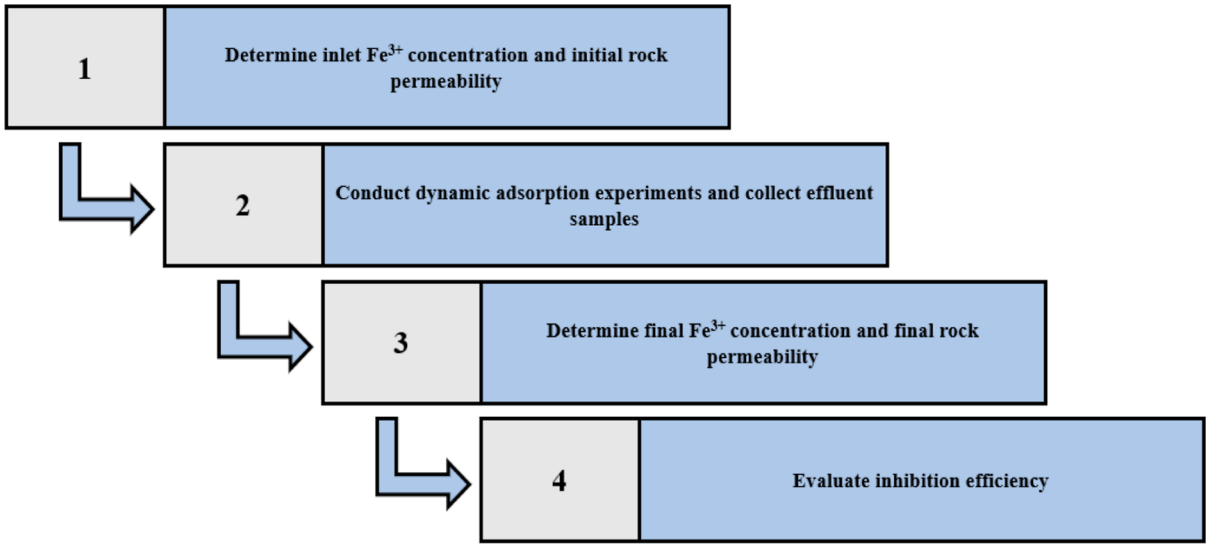

Figure 1. Flow chart detailing the stages of the inhibitor adsorption experiment.

https://doi.org/10.1021/acsomega.2c01568
ACS Omega 2022, 7, 26137−26153

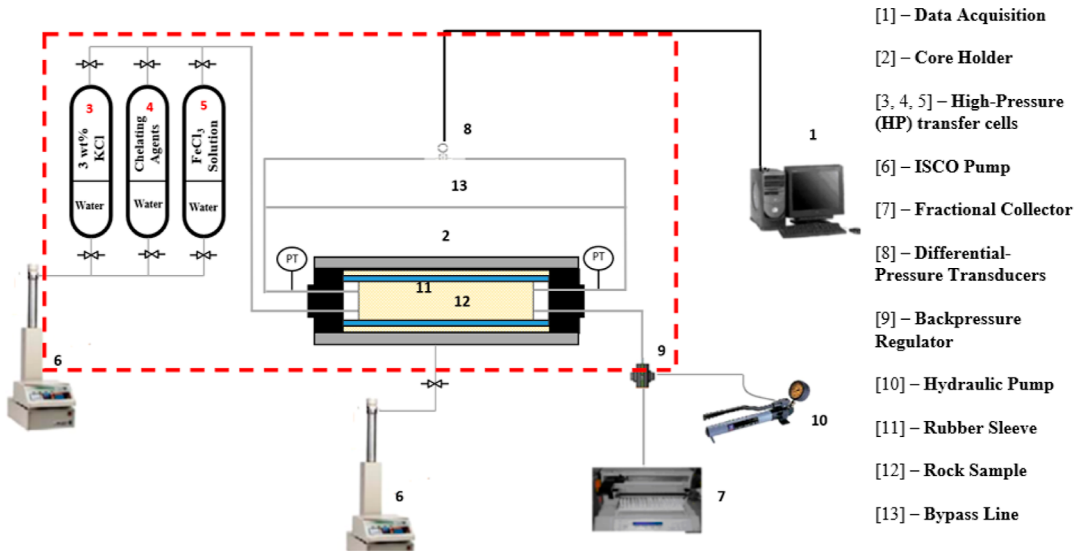

Figure 2. Coreflooding setup for dynamic adsorption experiments (photograph courtesy of "M.M.". Copyright 2011).

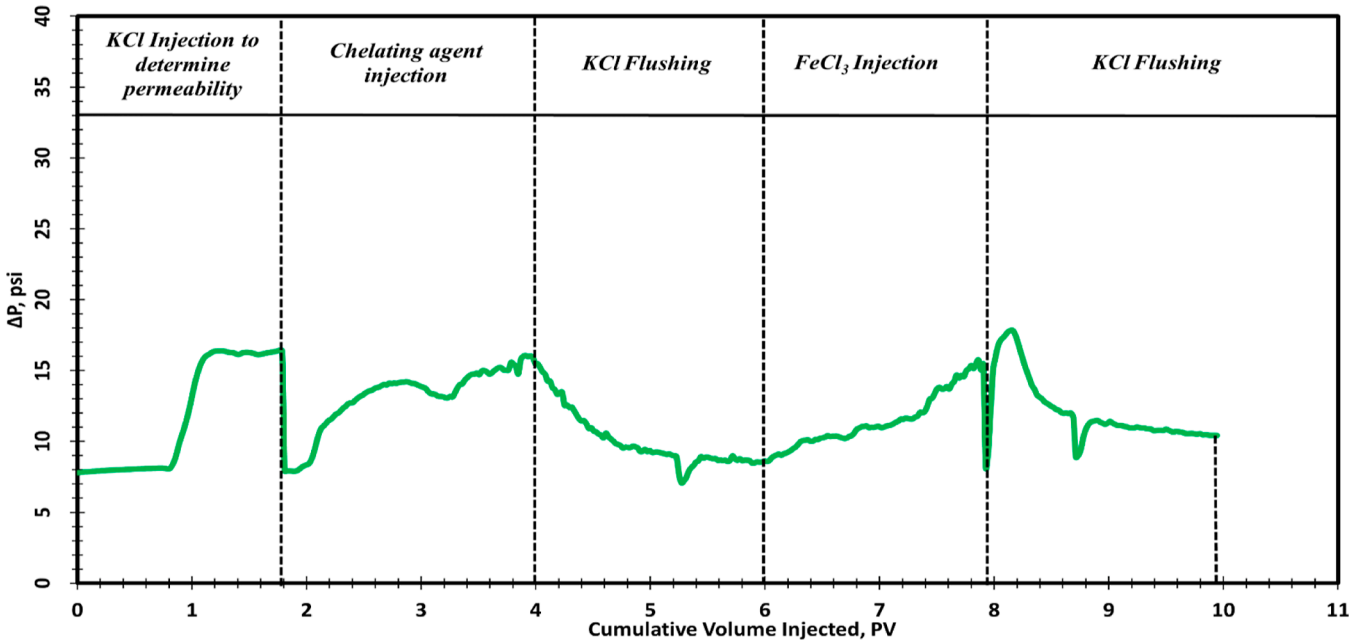

Figure 3. Injection sequence of the fluids for adsorption experiments.

Table 4. Conditions Used in Adsorption Experiments

coreflooding conditions	values
backpressure, psi	1000
confining pressure, psi	1500
flow rate, cm^3/min	0.5
temperature conditions, °C (°F)	25 °C (77 °F)

viscosity (viscosity of 3 wt % KCl = 1.002 cp) were then identified at room temperature. Finally, the PV of rock samples was calculated using eq 1.

$$V_{pore} = \frac{M_{wet} - M_{dry}}{\rho_{brine}} \quad (1)$$

Powdered calcite mineral was purified with deionized water (HPLC grade from Sigma-Aldrich) for ζ-potential measurements. The suspension was mixed using an orbital shaker for 24 h, after which insoluble particles were filtered and dried overnight at 80 °C (176 °F) in a vacuum oven. The salt solutions with concentrations of 0.1 and 1 M and different concentrations of ferric and ferrous solutions were freshly prepared.

10 mg of mineral powder was conditioned in a 30 mL buffer solution of changing pH (1−13) for 24 h before the measurements. The procedures were continued with preparing samples to analyze iron precipitation on the calcite mineral by mixing 1 mL of conditioned samples (pH 1−13) and 1 mL of iron solutions with varying Fe^{2+}/Fe^{3+} constituents. The mixtures were vibrated and allowed to maintain equilibrium before performing the measurements. Another set of sample preparation was done to study the effect of 0.1 and 1 M concentrations of salts (NaCl, $CaCl_2$, and $MgCl_2$) on Fe^{2+}/Fe^{3+} adsorption on the calcite particle surface following the same preparation procedures.

https://doi.org/10.1021/acsomega.2c01568
ACS Omega 2022, 7, 26137−26153

Experimental Methodology. Adsorption of chelating agents and the ability to chelate metal ions was determined by injection of $FeCl_3$ solution. Fe^{3+} crystals are highly prone to precipitate, and their deposition might influence the formation through either plugging of pore throats or solid precipitation due to interactions. The two mechanisms were studied by performing coreflooding experiments and ζ-potential measurements. The experimental workflow of the coreflooding experiments is shown in Figure 1. The core and fluid preparation was followed by determining the initial rock permeability by injecting 3 wt % KCl and measuring the ferric content in an injected $FeCl_3$ solution. The petrophysical properties of the core samples are reported in Table 3. Owing to possible errors in pressure readings and pump injection rates, the accuracy of permeability measurements is ±0.75%, and for porosity measurements, it is ±0.02%. The stabilized pressure drop value at varying constant flow rates was used to calculate initial rock permeability using the Darcy equation, as shown in eq 2.

$$k = \frac{122.812 q \mu L_{core}}{\Delta P d_{core}^2} \quad (2)$$

where q is the flow rate (cm^3/min), μ is the viscosity (cP), L_{core} is the length of the core sample (in.), ΔP is the pressure drop across the core (psi), d_{core} is the diameter of the core sample (in.), and k is the core permeability (mD).

The initial iron(III) concentration in injected ferric chloride solution was determined using inductively coupled plasma-optical emission spectrometry (ICP-OES). The underlying reason for tracking the ferric ions in the experiments is because ferrous ions can oxidize into the ferric form, particularly in water injection wells, and precipitate in the formation. Therefore, precipitation of iron(III) could result in the formation of iron-based scales.

Dynamic adsorption experiments were further performed, and the effluent samples were collected throughout the experiments. The capacity of IL cores adsorbing chelating agents was evaluated by utilizing a linear coreflooding setup by CoreLab and the Optima 8000 ICP-OES machine from PerkinElmer. The equipment has a novel optical system called a double monochromator having a dynamic wavelength stabilization system. The system can accurately travel the extremes of wavelength in the range of 160−900 nm. ICP-OES analyzes the photons emitted by excited atoms after losing their energy and returning to their original state. Peristaltic pumps are used to introduce the diluted effluent solution into the system. A system nebulizer converts the solution into a fine aerosol. The different atomic species within the aerosol are then excited by a plasma source. Argon gas ionized with a high concentration of electrons carries the plasma heat current at over 6000 K. ICP software determines what elements are present in the sample based on the standard emission intensity and the corresponding concentration. By knowing the initial and the final ferric concentrations in the injected ferric solution and effluent samples, the inhibition efficiency (adsorption) can be calculated using eq 3. Inhibition of ferric ions indicates the degree of adsorption. The adsorption of more chelating agents results in fewer ferric ions in effluent samples, which indicates the amount of adsorption.

$$\text{Inhibition efficiency} = \frac{\text{inlet } Fe^{3+} \text{ concentration} - \text{maximum outlet } Fe^{3+} \text{ concentration}}{\text{inlet } Fe^{3+} \text{ concentration}} \quad (3)$$

The coreflooding setup incorporates three-piston HP transfer cells, a core holder, a confining pressure pump, an ISCO injection pump, pressure transducers, a backpressure regulator (BPR), and an electric oven. The coreflooding setup is pictured in Figure 2. The ISCO pump was used to maintain the required injection rate with the accuracy of ±0.5%. The pressure transducers are manufactured by CoreLab and have an accuracy of ±0.25% in determining pressure readings on the core inlet and outlet sections. The operational limits of ISCO pumps were a maximum flow rate of 50 cm^3/min and a pressure of 7500 psi. The BPR (BP-100-SS) from CoreLab was used in the coreflooding to maintain constant back pressure in the system. The working pressure of the regulator is up to 10,000 psi, and the temperature is up to 350 °F. The automatic fractional collector—Gilson 223—was used to constantly collect the effluent samples within the desired time period. The pressure transducers are installed on the inlet and outlet sides of the core holder for the determination of the differential pressure across the core sample. The main reason for using the bypass line is to build up the pressure on the outlet and inlet section simultaneously and to clean the unnecessary fluids from the production line in order to produce new fluid from the core sample.

The final iron(III) concentration in effluent samples was measured using ICP-OES. The final permeability of the core samples was obtained utilizing coreflooding. The final stage was evaluating the inhibition efficiency of chelating agents (EDTA and DTPA) and the degree of formation damage ($k_{final}/k_{initial}$) due to ferric precipitation.

The fluid injection sequence of the adsorption experiments with an approximate pressure drop across the core is depicted in Figure 3.

The temperature, pressure conditions, and flow rate in which the coreflooding experiments were conducted are indicated in Table 4. The backpressure was chosen to be 1000 psi to maintain the resisting pressure to the flow and produce realistic near-wellbore conditions, and the overburden pressure representing reservoir conditions was chosen to be 1500 psi. The lower flow rate (0.5 cm^3/min) was used to achieve reasonable chelating agents' adsorption considering the near-wellbore stimulation treatment. The flow rate is considered as high rate if the main focus of the work is EOR treatments.

The electrostatic interaction between Fe^{2+}/Fe^{3+} particles and calcite mineral particles (solid/solid) at varying pH environments was analyzed by performing a series of ζ-potential measurements. Through the production life of the wells, various operations cause alteration of the reservoir environment (pH), which influences the surface charge of the rocks. This pH variability changes the surface chemistry of minerals, which causes problems, such as wettability alteration and scale precipitation. Therefore, the fundamental idea behind performing the measurements is to understand the iron precipitation in calcite minerals in a wide range of pH environments.

X-ray diffraction was performed using a diffractometer with a Cu source by Malvern Panalytical to identify the mineralogy of the particles. The calcite mineral consists of 99.7% calcite and 0.3% quartz. The Malvern Zetasizer Nano Z was utilized to

https://doi.org/10.1021/acsomega.2c01568
ACS Omega 2022, 7, 26137−26153

conduct ζ potential (ZP) measurements on samples in the electrolytic solution. The measurements were performed with three repetitions, and the standard deviation between the run was in the range of 0.32 and 2.53 mV considering all the measurements. The method of laser doppler electrophoresis was used to determine ZPs of colloidal suspensions, and the application of a voltage across a cell determined particle mobility, which was used to calculate the particle ZP using the Henry equation (eq 4)[31,32]

$$U_E = \frac{2E\zeta f(kR)}{3\eta} \quad (4)$$

where ζ is the ZP, E is a dielectric constant, η is the viscosity, U_E is the electrophoretic mobility, and $f(kR)$ is Henry's function.

RESULTS AND DISCUSSION

Adsorption Experiments. The adsorption experiments were performed to evaluate the adsorption capacity of limestone core samples using coreflooding and ICP-OES. The effect of the type, concentration, soaking time of chelating agents, and the addition of salts on chelating agent adsorption was studied. The permeability alteration was further calculated for quantifying the formation damage. The injected ferric solution contained 2800 ppm of Fe^{3+} ions. It is necessary to mention that the adsorption of chelating agents was tried to achieve within the near-wellbore damage radius (approximately 3 ft), as shown in Figure 4. The injected PV at a radial distance of r_{damage} is one PV for 3 ft.[33] The main attention is on water injection wells where there is no significant oil presence in the near-wellbore region. However, the inhibitors can be injected into the formation using different oil solvents to avoid oil deposits in this region.

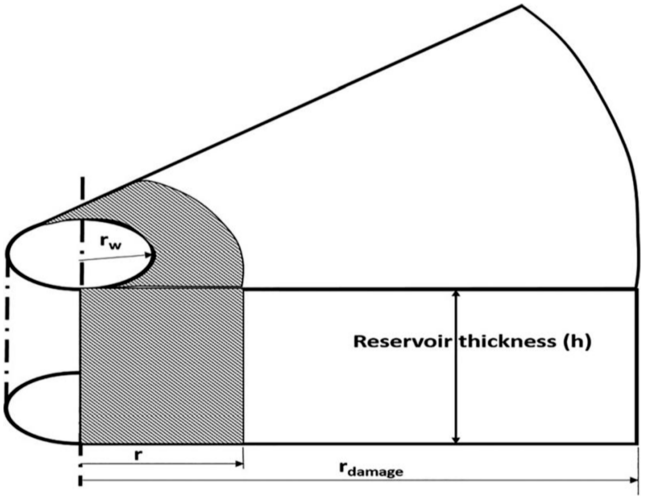

Figure 4. Schematic representation of the damage radius of 3 ft[33] (adapted with the permission of publisher, M.M., 2017, from doi.org/10.1115/1.4036251).

The experiment was conducted without any chelating agent to determine the formation damage due to the ferric precipitation and natural iron(III) adsorption capacity of the IL-1 core sample at an ambient temperature condition. Figure 5 illustrates the pressure drop profile and the change in the ferric concentration during the experiment. The pressure drop increased up to 150 psi after $FeCl_3$ injection attributed to the precipitation of iron(III) particles causing pore throat plugging. The maximum Fe^{3+} concentration based on the effluent samples was 1744 ppm, which yielded a calculated natural adsorption of 38%. The final permeability was 9.9 mD, and the resulting permeability decrease was 50%. Questioning the reproducibility of the permeability measurements, the initial and final permeability of the rock samples were determined several times to validate the reported permeability values. The delay in Fe^{3+} production in the experiments is due to the sequential injection process, and the KCl within the injection lines is still injected across the core sample for some early period of $FeCl_3$.

Then, adsorption of 10 wt % EDTA using the IL-2 core sample was carried out. Before injecting a ferric solution, 10 wt % EDTA was injected into the core. Figure 6 depicts a change in the pressure drop and iron(III) concentration during the adsorption of 10 wt % EDTA. Based on the results of ICP-OES measurements, the maximum Fe^{3+} concentration was indicated as 550 ppm, and 10 wt % EDTA was able to reduce the ferric concentration from 2800 ppm to a maximum of 550 ppm, resulting in 80% inhibition efficiency that attributed to adsorption of 10 wt % EDTA. Furthermore, the final to the initial rock permeability ratio was found to be 0.77, which implies the reduction of permeability by 23%. The results revealed that adsorption of 10 wt % EDTA had a profound positive effect on damage due to ferric precipitation and complexes 2250 ppm of Fe^{3+} ions.

IL-3 and IL-4 core samples were used for the experiments to encounter the possible influences of Ca^{2+} and Mg^{2+} cations on 10 wt % EDTA on adsorption. The mixtures of 10 wt % EDTA with 5000 ppm of $CaCl_2$ and $MgCl_2$ by maintaining a pH of 11 were prepared. The inhibition efficiency of 10 wt % EDTA decreased with Mg and Ca salts. The phenomenon might be due to the low concentration of mixed salts.[3]

The pressure drop across the core samples and ferric concentration variation is represented for $CaCl_2$ and $MgCl_2$ in Figures 7 and 8, respectively. The highest determined Fe^{3+} concentration was 1222 ppm resulting in an inhibition efficiency of 56% in the case of $CaCl_2$, while in the treatments with 10 wt % EDTA mixed with $MgCl_2$, the maximum iron(III) concentration was found to be 1335 ppm with an inhibition efficiency of 52%. The $k_{final}/k_{initial}$ was ascertained as 0.56 and 0.50, respectively.

The adsorption of 15 and 20 wt % EDTA was examined using IL-7 and IL-8 core samples. The change in the Fe^{3+} concentration as a function of the cumulative injected volume using 15 and 20 wt % EDTA is illustrated in Figure 9A,B, correspondingly. The achieved inhibition efficiency of 15 wt % EDTA was 70%, whereas 20 wt % EDTA produced 84% inhibition efficiency. The permeability of both rock samples was reduced by 26%.

Based on the obtained results, the best-adsorbed EDTA concentration was 20 wt %. The effect of the soaking time of 1 h (hour) and 2 h was further analyzed using 10 wt % EDTA. The adsorption of 10 wt % ETDA did not significantly change with an additional 1 h of soaking time. Furthermore, 2 h of soaking time was examined with both 10 and 20 wt % EDTA. IL-5 and IL-6 core samples were used for 10 wt % EDTA for 1 and 2 h, respectively. The IL-9 core sample was used for the experiment with 20 wt % EDTA having a soaking time of 2 h. Figure 10 represents the inlet ferric concentration and the highest observed outlet ferric concentrations.

https://doi.org/10.1021/acsomega.2c01568
ACS Omega 2022, 7, 26137−26153

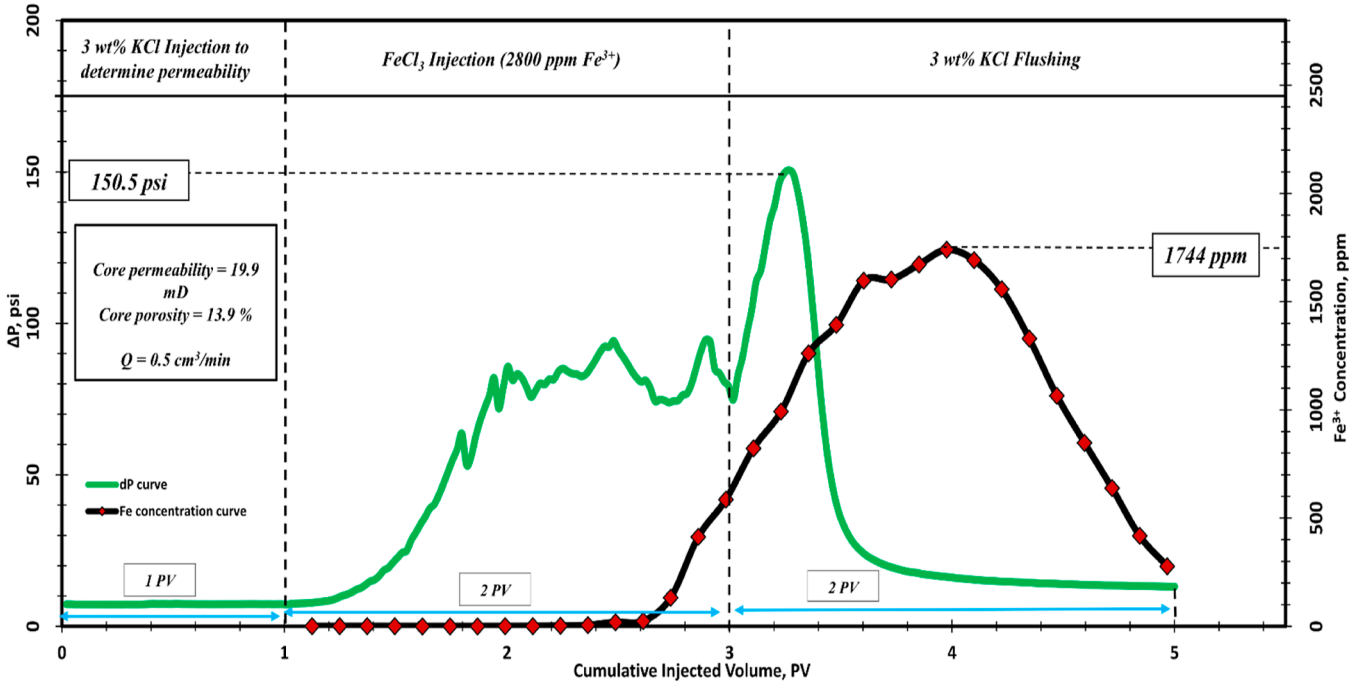

Figure 5. Pressure drop across the core (IL-1) and iron(III) concentration at 25 °C (77 °F) (without inhibitor).

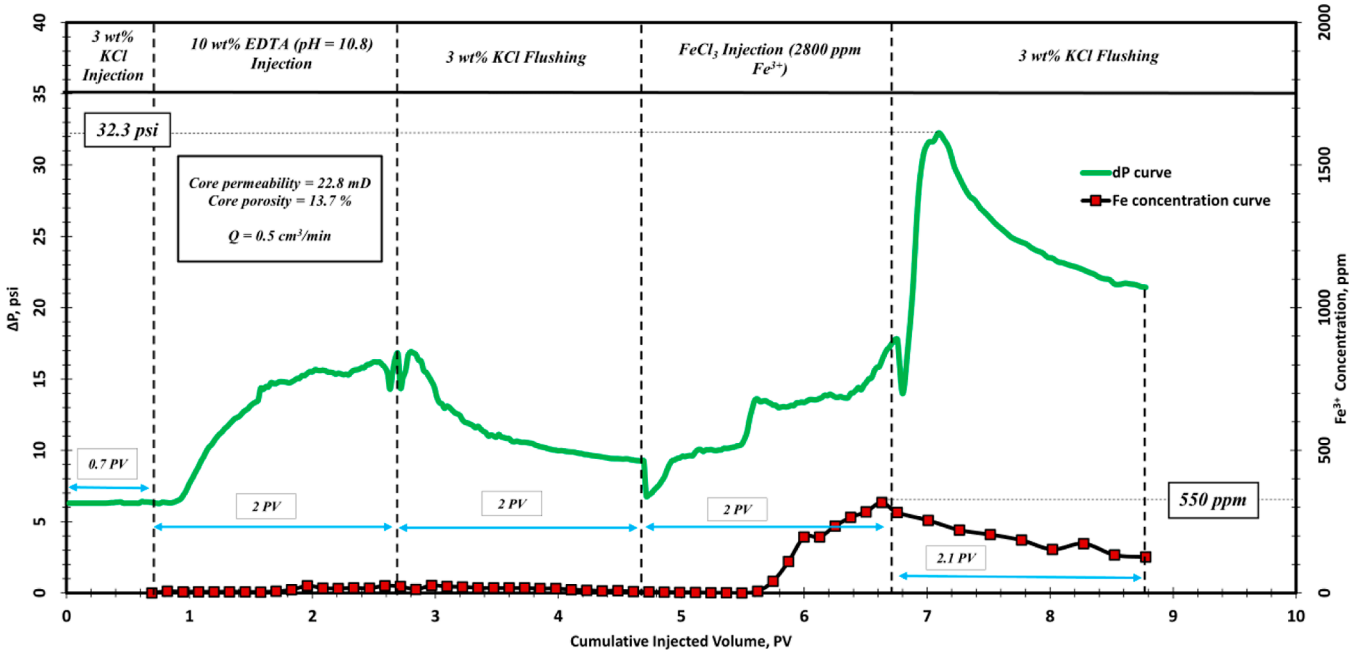

Figure 6. Pressure drop across the core (IL-2) and iron(III) concentration at 25 °C (77 °F) (10 wt % EDTA).

Compared to 10 wt % EDTA, 28 ppm less Fe^{3+} was observed in effluent samples, in the case of 1 h of soaking time, while 2 h of soaking time resulted in chelation of 61 ppm more of Fe^{3+}. These results revealed that 1 and 2 h of soaking time for 10 wt % EDTA to be adsorbed in the core sample resulted in 81 and 83% inhibition efficiency yielding 1 and 3% of more adsorption, respectively. Similarly, 2 h of soaking time for 20 wt % EDTA resulted in 86% inhibition efficiency, with 2% more inhibition than 20 wt % EDTA. The inhibition efficiencies that correspond to the effect of soaking on chelating agent adsorption are summarized in Figure 11. Figure 12A compares the permeability alteration for 10 wt % EDTA, and the permeability reduction was 23 and 21%, respectively. This trend also proves that the impact of 1 and 2 h soaking time was not profound in 10 wt % EDTA. The same phenomenon was observed with 20 wt % EDTA (Figure 12B).

After evaluating the adsorption of different EDTA concentrations, an adsorption experiment was performed using DTPA with the optimum concentration obtained from EDTA adsorption tests. DTPA and EDTA both show relative stability and inhibition efficiency against ferric ions at an ambient temperature.[34] The adsorption of 20 wt % DTPA was analyzed on the IL-10 core sample. 20 wt % DTPA showed an

https://doi.org/10.1021/acsomega.2c01568
ACS Omega 2022, 7, 26137−26153

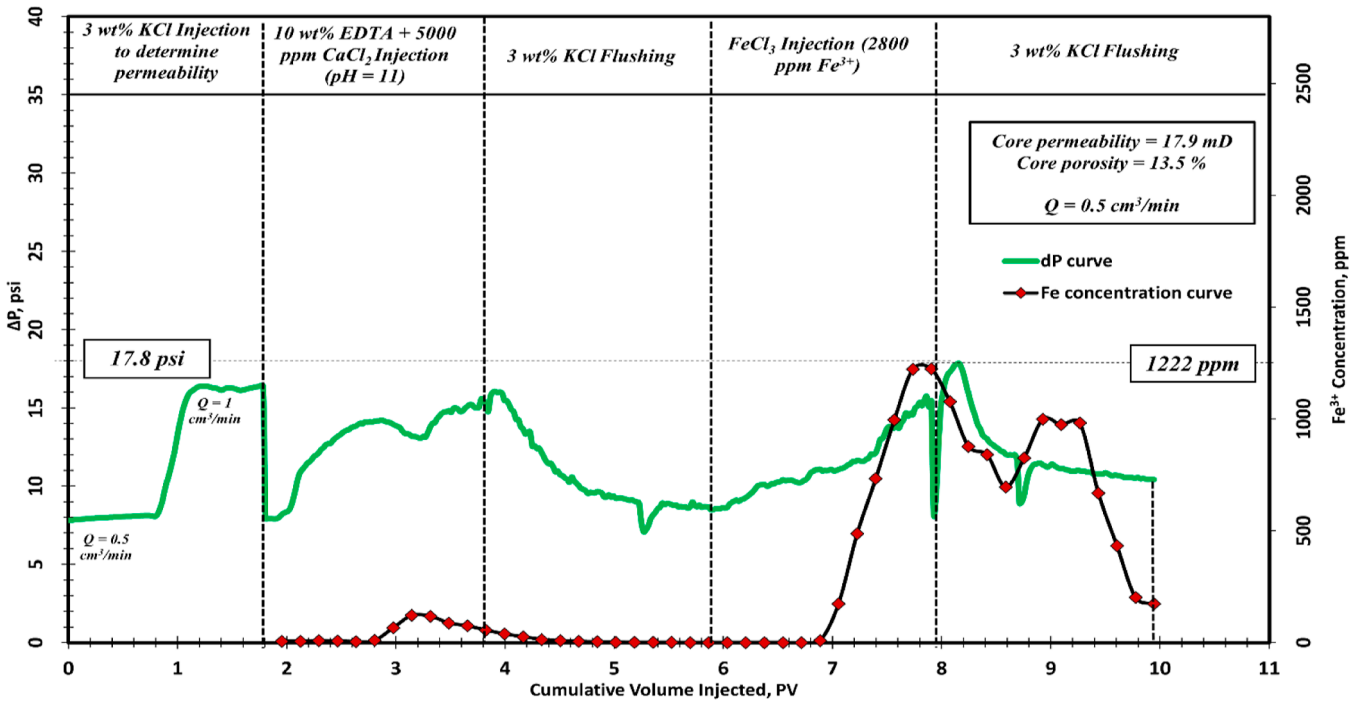

Figure 7. Pressure drop and Fe^{3+} concentration during the experiment using 10 wt % EDTA with Ca^{2+} at 25 °C (77 °F).

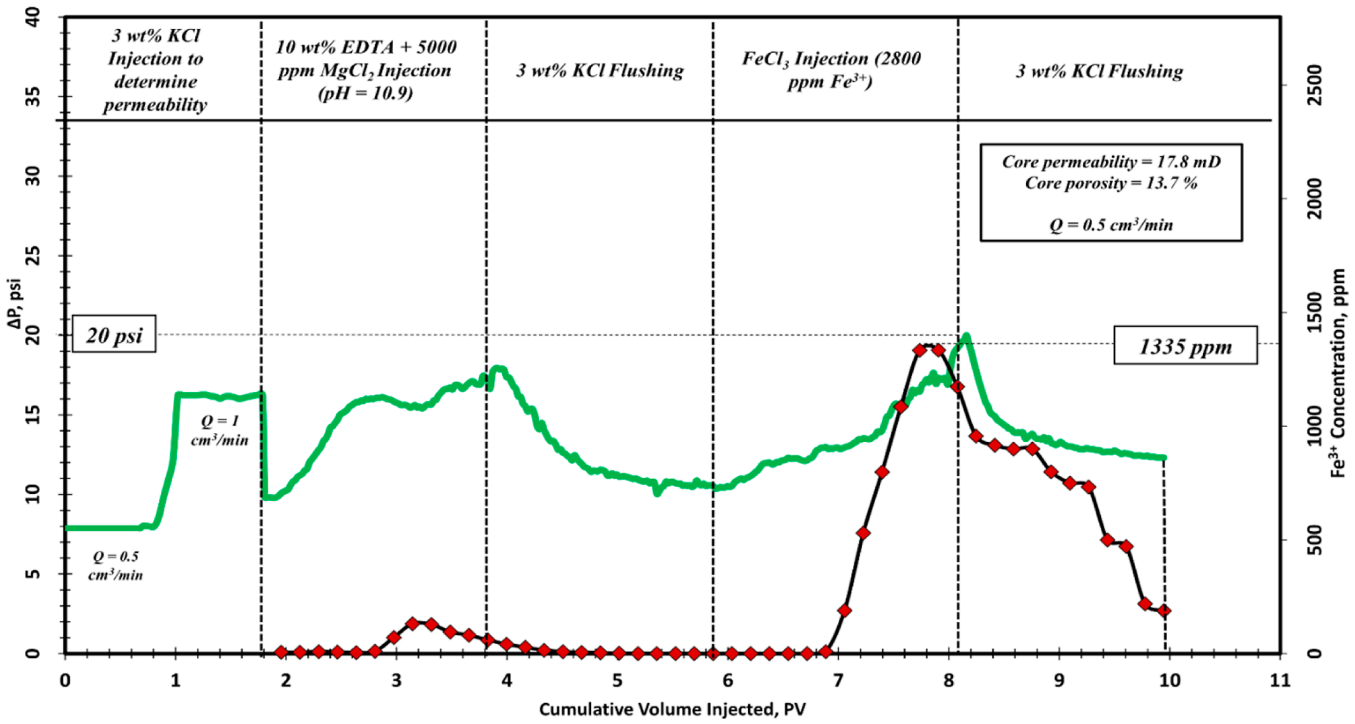

Figure 8. Pressure drop and Fe^{3+} concentration during the experiment using 10 wt % EDTA with Mg^{2+} at 25 °C (77 °F).

inhibition efficiency of 85% (Figure 13), and the permeability reduction was determined as 32% (Figure 14).

Summary of Adsorption Experiments. 20 wt % EDTA and 20 wt % DTPA proved to have the highest adsorption capacity and more effectively complex ferric ions at an ambient temperature condition based on the adsorption experiments. Figure 15A summarizes the inhibition efficiency obtained from dynamic adsorption experiments. Figure 15B represents the permeability reduction due to ferric precipitation. 20 wt % EDTA inhibited 84% of Fe^{3+} ions, and permeability reduction was 26%. 20 wt % DTPA, in turn, resulted in 85% inhibition efficiency, and permeability diminished by 32%.

Figure 16 shows the relationship between the inhibition efficiency and the determined maximum ferric concentration during adsorption experiments. The graph identifies the best-adsorbed concentration considering the fact that the permeability reduction for EDTA and DTPA is comparable. The relationship also shows that the optimum EDTA

https://doi.org/10.1021/acsomega.2c01568
ACS Omega 2022, 7, 26137−26153

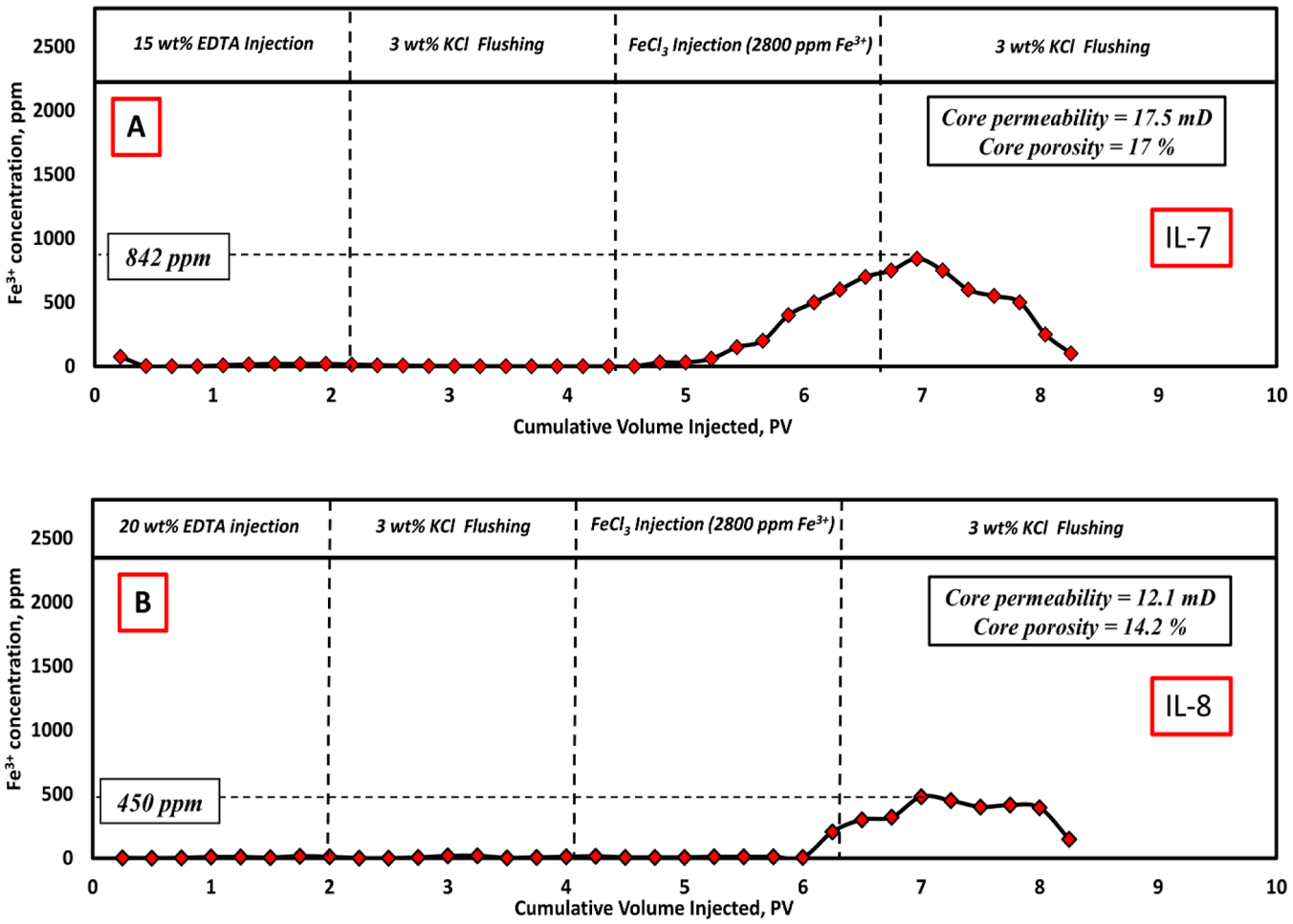

Figure 9. Fe^{3+} concentration during the coreflooding experiment using 15 and 20 wt % EDTA at 25 °C (77 °F). (A) 15 wt % EDTA and (B) 20 wt % EDTA.

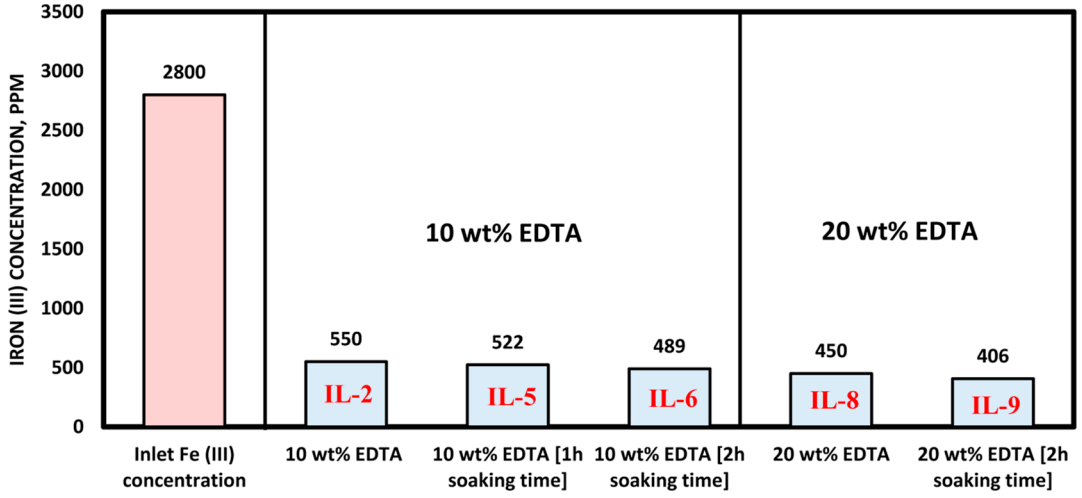

Figure 10. Initial and maximum final Fe^{3+} concentrations (with and without soaking time).

concentration that produced the highest adsorption is 20 wt %. Moreover, 20 wt % DTPA has 1% more inhibition efficiency compared to 20 wt % EDTA, but considering the economic factor, EDTA is a more economically viable selection compared with DTPA.[35]

The adsorption experiments revealed that a higher concentration of the chelating agents produces more adsorption at ambient temperature conditions in calcite minerals by the complexation of more iron(III) ions. The adsorption of chelating agents and their ability to capture ferric ions is influenced by the presence of the salts in the system. Therefore, low concentrations of the $CaCl_2$ and $MgCl_2$ salts decreased the amount of iron(III) captured by the chelating agent and decreased the adsorption. However, the soaking

https://doi.org/10.1021/acsomega.2c01568
ACS Omega 2022, 7, 26137−26153

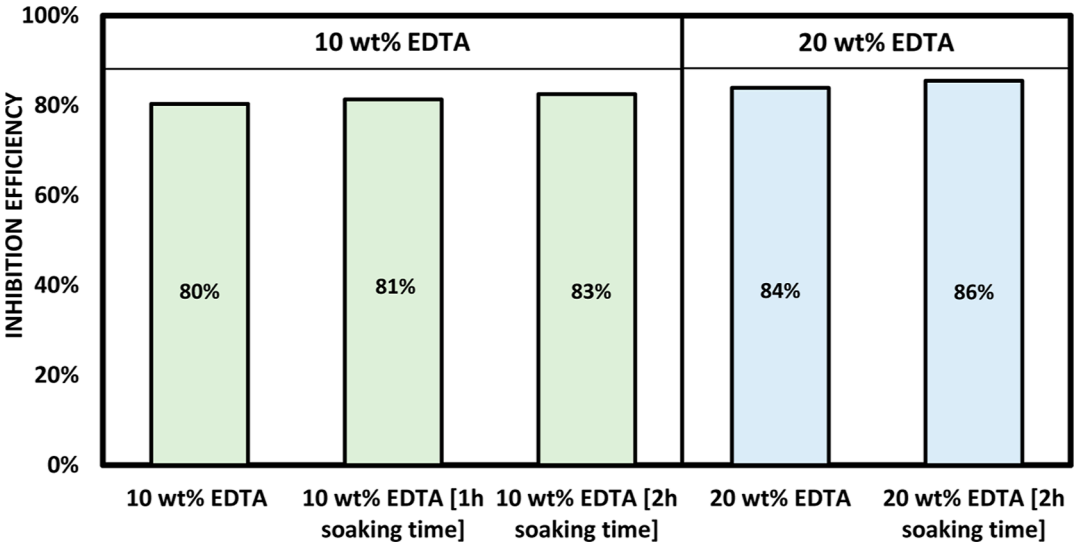

Figure 11. Comparison of inhibition efficiencies (without/with soaking time).

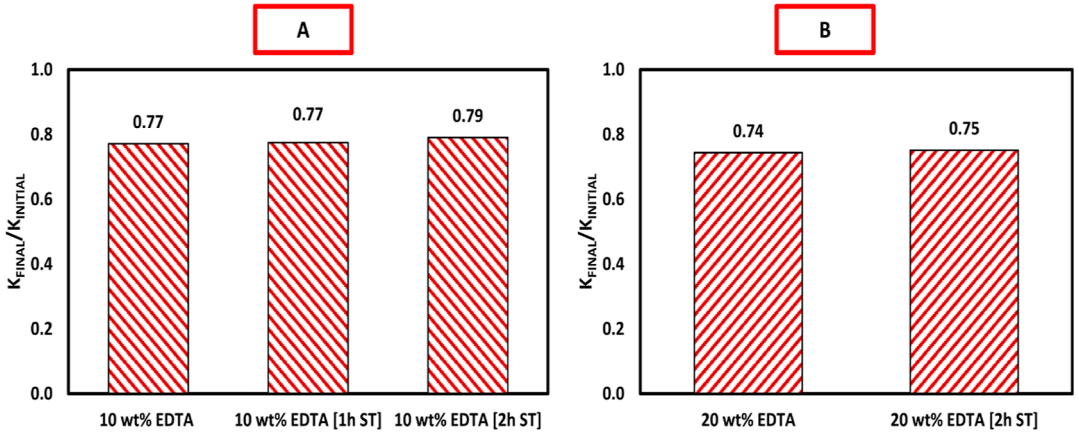

Figure 12. Permeability change K_f/K_i. (A) 10 wt % EDTA and (B) 20 wt % EDTA.

time of inhibitors comparably increased the adsorption of the chelating agents and complexed more iron ions from the aqueous solution.

ζ-Potential Measurements. Chemical interactions that take place during different well operations significantly affect the pH environment of the reservoir formation and cause precipitation of solid crystals of various scales. The ZP values of calcite minerals in pH environments from 1 to 13 were first determined. The trend of surface charge alteration of the calcite minerals replicated the results of previous studies on calcite minerals in the literature.[30,36] Charge development of calcite minerals is a vital function of the pH environment.[37,38] Five sets of ZP measurements were conducted. In addition, the precipitation of different concentrations of ferrous and ferric ions on calcite minerals was further evaluated. Figure 17 illustrates the calcite mineral surface charge and the impact of iron(III) and iron(II) charge development of calcite.

It is observed that there is an increase in the negative charge in the acidic region (pH 1−4) that could be attributed to protonation of the calcite mineral (base case). The reduction in the ZP value from pH 4 to 7 can be because of a double-layer compression. Between pH values 7 to 8, Gary et al.[39] and Heberling et al.[40] reported that such fluctuation in the surface charge is due to the slow dissolution of the calcite mineral. It is found that there is a double-layer collapse, while from 8−12, the further decrease might be because of adsorption of OH^- on the calcite particle surface. OH^- adsorption within this pH range is also reported by Mohammed et al.[30] and Al Mahrooqi et al.[36] The compression of the double layer can be the reason for behavior in the pH range of 12−13.

ZP values between −5 and 5 mV (the red-dotted region in ZP figures) indicate a high possibility of instability and particle precipitation. Five different concentrations of iron(III) were chosen to study the precipitation of ferric ions. Fe^{3+} ions are typically prone to precipitate once the pH of the system becomes 1.[41,42] Ferric concentrations were grouped into two categories in which ferric concentrations were lower than 1600 ppm (Figure 17A) and higher than 5000 ppm (Figure 17B). It is evident that the iron(III)-containing system showed a higher ZP with around −10 and 10 mV in some pH values. However, it can be concluded that regardless of the iron(III) concentration, iron(III) ions precipitate on the calcite surface in the whole range of pH environments. Therefore, unstable behavior becomes inevitable for the higher ferric concentrations, and higher concentrations result in more obvious ferric precipitation on the calcite mineral surface.

The precipitation of ferrous ions was evaluated using six different concentrations of iron(II). Unlike ferric ions, it is

https://doi.org/10.1021/acsomega.2c01568
ACS Omega 2022, 7, 26137−26153

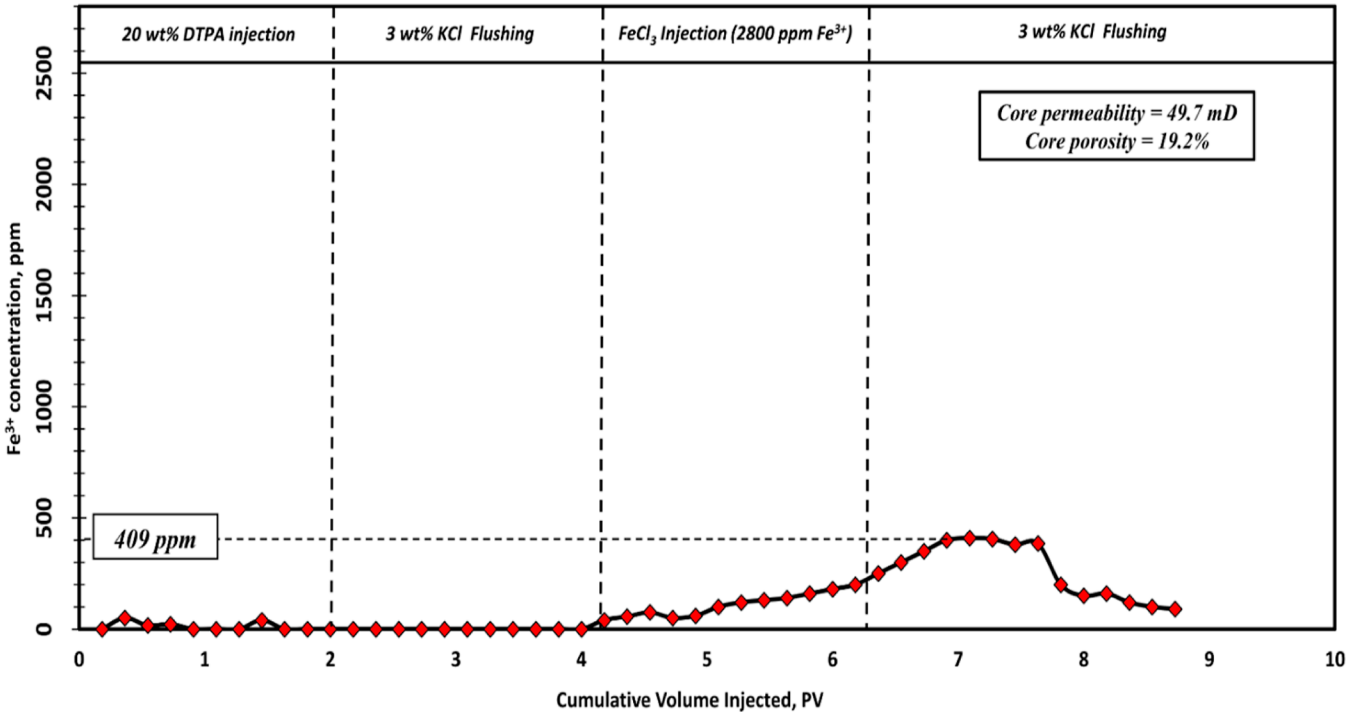

Figure 13. Fe^{3+} concentration during the coreflooding experiment using 20 wt % DTPA at 25 °C (77 °F).

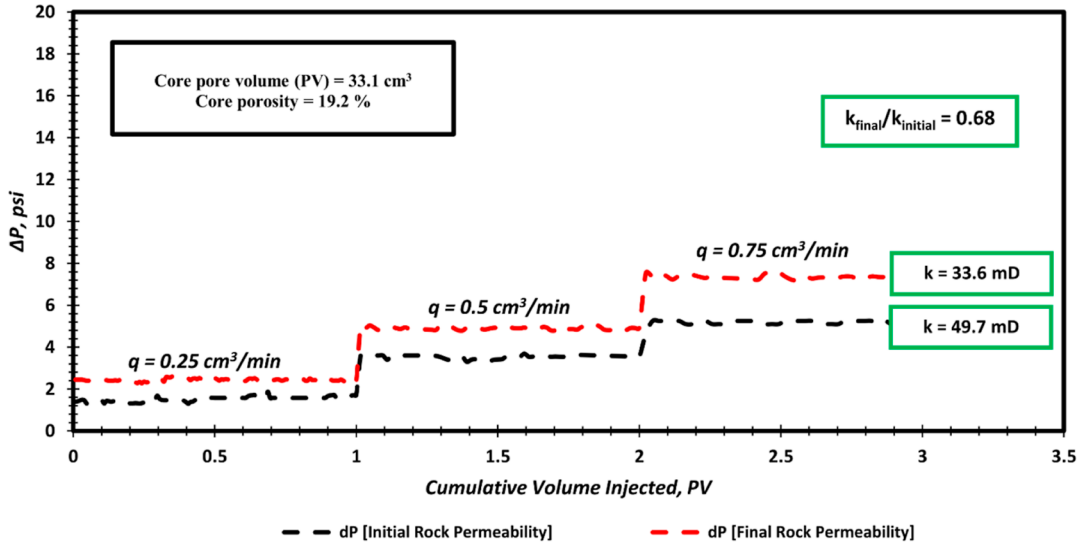

Figure 14. Permeability alteration K_f/K_i (20 wt % DTPA).

reported that ferrous ions usually start to precipitate in pH environments higher than 6.[42] The concentrations of ferrous ions were divided into two categories. In the first category, the iron(II) concentration was lower than 1600 ppm (Figure 17C), whereas ferrous concentrations were higher than 3000 ppm in the second category (Figure 17D).

The low concentrations of ferrous ions did not result in high precipitation on calcite minerals. In the case of 100 ppm, it is apparent that there is a fluctuation between positive and negative surface charges. In comparison, as the concentration of ferrous increases toward 500 and 1500 ppm, the system becomes predominantly positively charged. A 100 ppm ferrous concentration shows ZP values very close to zero potential charges in pH environments from 1 to 2 and 4. However, having more ferrous ions in the system in the acidic region resulted in higher ZP values. The variation of ZP values for the second criteria, which includes Fe^{2+} concentrations higher than 3000 ppm, is shown in Figure 17D. The phenomenon of dominance by positive charges continued for 3000 ppm or higher concentrations of ferrous. Obviously, in the pH environments higher than 6, there is a declining trend of ZP values toward the zero potential charge with the only exception of the pH region of 11−13 for 3000 ppm of Fe^{2+}. This trend shows that, unlike ferric ions, the concentration of ferrous ions impacts the stability of the system. A higher concentration of ferrous in the system gives more instability and lower ZP values. On the other hand, lower concentrations of ferrous ions show erratic changes in ZP charges on the calcite surface charge development.

https://doi.org/10.1021/acsomega.2c01568
ACS Omega 2022, 7, 26137−26153

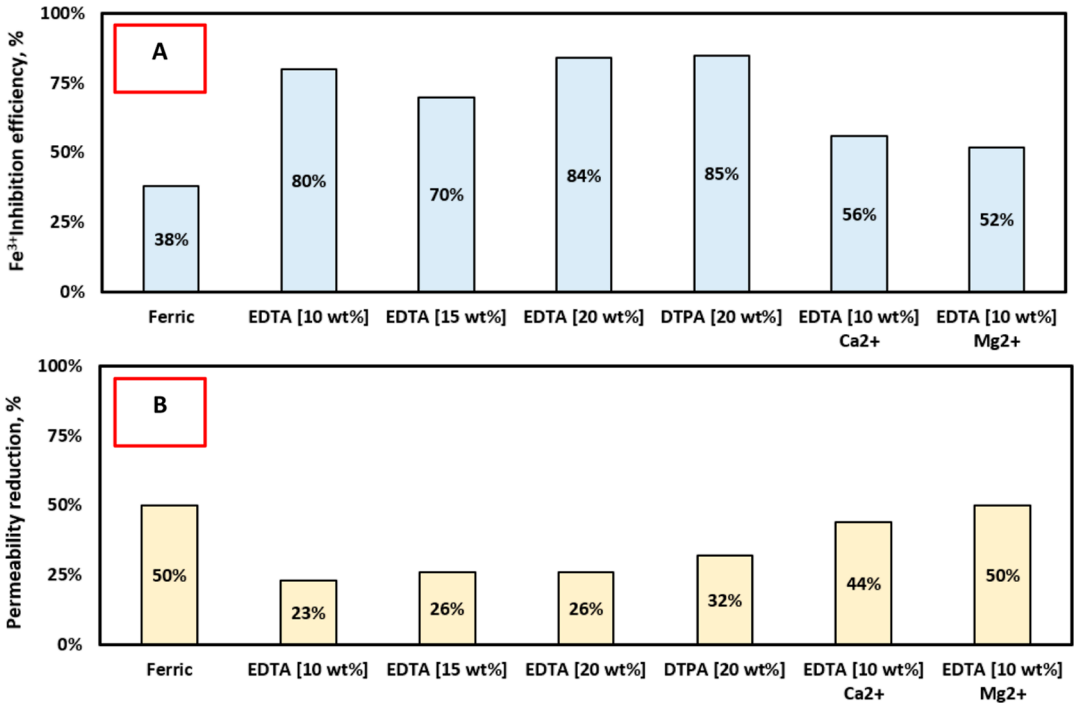

Figure 15. Summary of adsorption experiments. (A) Inhibition efficiency and (B) permeability reduction.

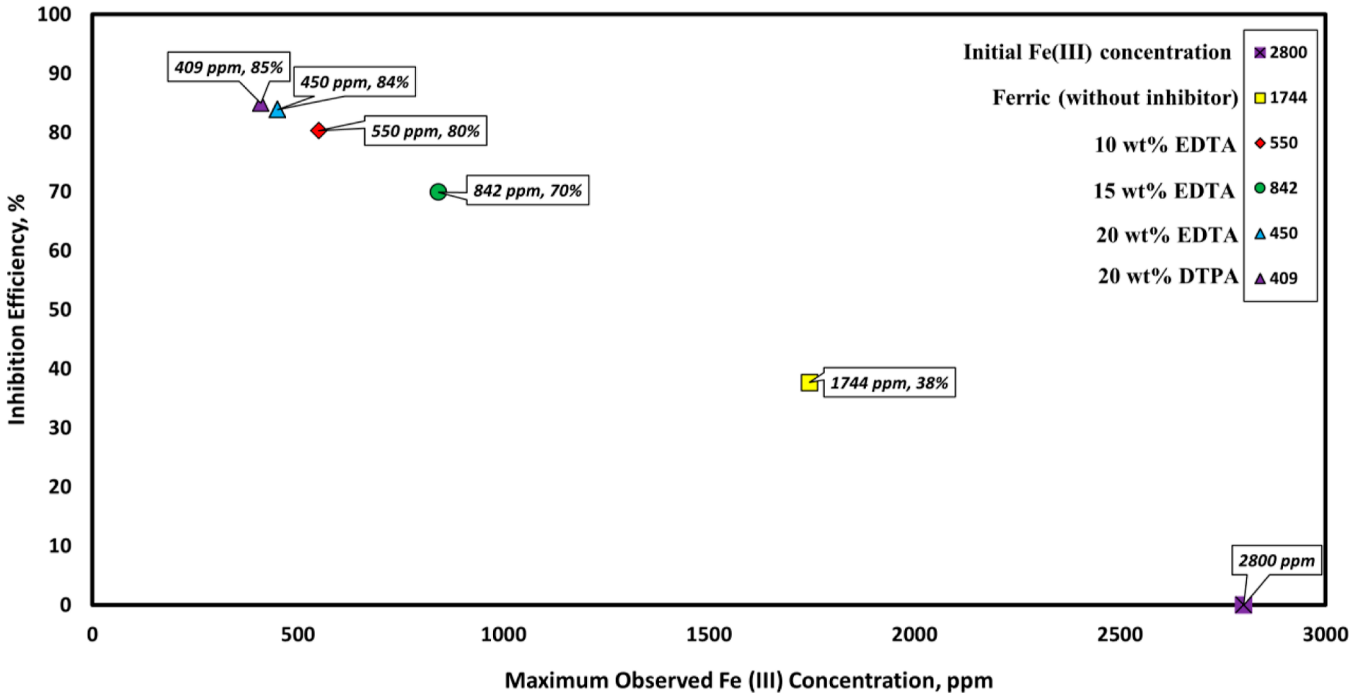

Figure 16. Graph determining the optimum chelating agent concentration.

Afterward, ZP measurements were conducted to determine the interaction of calcite minerals with 0.1 and 1 M of NaCl, $MgCl_2$, and $CaCl_2$ salts. Figure 18 shows calcite mineral charge development with the addition of the three salts in the system.

0.1 M NaCl represents almost the same trend with the calcite mineral and is shown in Figure 18A. However, at pH 5−7, a double-layer compression can be observed from the trend. Hence, it can be concluded that in the charge development of calcite minerals, 0.1 M NaCl does not have a considerable influence. In contrast, the 1 M NaCl solution impacted ZP values producing a more stable system and changing the system into a negative charge-dominated system. There is an interchanging of the surface charge in the high pH, alkaline region. This can be explained by the adsorption of OH- competing with a double-layer collapse and double-layer compression from pH 12 to 13. The ZP charge trend for NaCl is also well-matched with Mohammed et al.[30] and Jackson et al.[43] as a low concentration of NaCl produced a more negatively charged system, while a higher concentration resulted in a more positively charged system.

https://doi.org/10.1021/acsomega.2c01568
ACS Omega 2022, 7, 26137−26153

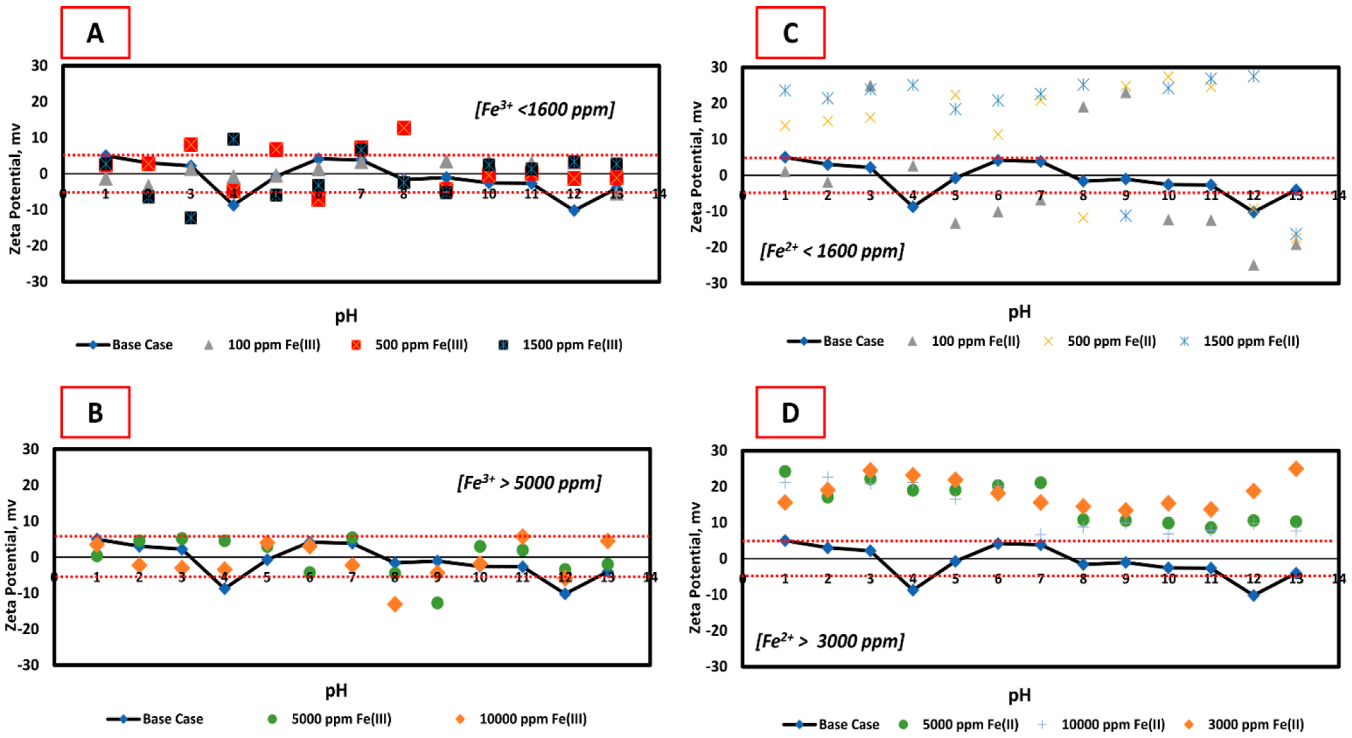

Figure 17. Effect of iron(II) and iron(III) on the calcite ZP. (A) Low Fe (III) concentrations, (B) high Fe (III) concentrations, (C) low Fe (II) concentrations, and (D) high Fe (II) concentrations.

Calcite mineral interactions with 0.1 M $MgCl_2$ and 1 M $MgCl_2$ were analyzed and are shown in Figure 18B. The trend (0.1 M $MgCl_2$) indicates that Mg^{2+} cations might adsorb on the mineral surface. A slight decrease in very high acidic regions might be due to the compression of a double layer. Concerning the base calcite case, it can be seen that there is a slight increase in a highly alkaline environment, which can be the result of OH^- adsorption on the mineral surface. The tendency also shows interchanging of ZP charges at pH 8−13. The system becomes more stable, and the ZP values support this idea in almost all pH environments, except the pH range between 6 and 9 in the case of 1 M $MgCl_2$. 1 M $MgCl_2$ generates a negatively charged system in the acidic region, followed by a double-layer compression at pH 3−4, while a double-layer collapse occurred in pH environments from 10 to 13.

The effect of $CaCl_2$ on the charge development of calcite minerals is represented in Figure 18C. 0.1 M $CaCl_2$ imitates the behavior of 0.1 M $MgCl_2$. A low concentration of $CaCl_2$ did not significantly impact the change in the surface charge of calcite minerals, whereas 1 M $CaCl_2$ influenced the calcite ZP charge by forming a more stable system in a near-neutral pH environment (5−6) and a slightly alkaline environment (8−10). Between pH 4 and 5 and 7 to 9, there is a double-layer compression,[44] while at pH 6 to 7, a double-layer collapse occurs. The results for divalent salts are within the agreement with Nande and Patwardhan,[45] and it was claimed that a low concentration of $MgCl_2$ and $CaCl_2$ resulted in a less positively charged or entirely negatively charged system, while a higher salt concentration gives more of a positively charged surface.

The impact of 0.1 and 1 M salt solutions on ferric precipitation was investigated. Two concentrations of ferric solutions (1500 ppm Fe^{3+} and 10,000 ppm Fe^{3+}) were chosen for the analyses. The results were analyzed from the perspective of iron(III) precipitation. Figure 19A,B depicts calcite surface charge development in the case of 1500 ppm of ferric ions, while Figure 19C,D represents the system containing 10,000 ppm of Fe^{3+}.

For 1500 ppm of the Fe^{3+} concentration, it is obvious from Figure 19A that a low concentration of NaCl produces an even higher degree of instability and triggers precipitation except in pH 6, where NaCl makes the system more stable. Unlike 0.1 M NaCl, in acidic regions and near-neutral pH environments, 1 M NaCl creates a more stable system, whereas in the pH environments between 10 and 13, the near-zero potential charge trend continues (Figure 19B). Figure 19C illustrates how 0.1 M NaCl influenced the ZP value of the calcite system that involves 10,000 ppm Fe^{3+}. The results reveal that 0.1 M NaCl affects Fe^{3+} behavior as it forms an almost negatively charged and more stable system at pH 2, 5−6, and 11−13. However, the effect of 1 M NaCl on the same system creates positively charged systems at pH 2−5 and pH 7−11. The system shows a high stability at pH 2−3 and 7−9, while 1 M NaCl results in ferric precipitation in highly alkaline regions (Figure 19D). According to the results, in a relatively low concentration of Fe^{3+}, 0.1 M NaCl almost did not affect charge development of calcite, while 1 M NaCl had an impact on ferric precipitation. However, at a high concentration of Fe^{3+}, both 0.1 M NaCl and 1 M NaCl promote significant surface charge development changes by creating negative charge dominant (0.1 M NaCl) and positive charge dominant (1 M NaCl) and a relatively stable system.

The measurements were followed by investigating the resulting alteration of the ZP charge due to 0.1 M MgCl2 and 1 M MgCl2 on the system containing 1500 ppm Fe^{3+} and 10,000 ppm Fe^{3+}. Figure 20B shows the outcomes of the measurements for 0.1 M $MgCl_2$ on a calcite system having 1500 ppm Fe^{3+}. According to the trends, 0.1 M $MgCl_2$

https://doi.org/10.1021/acsomega.2c01568
ACS Omega 2022, 7, 26137−26153

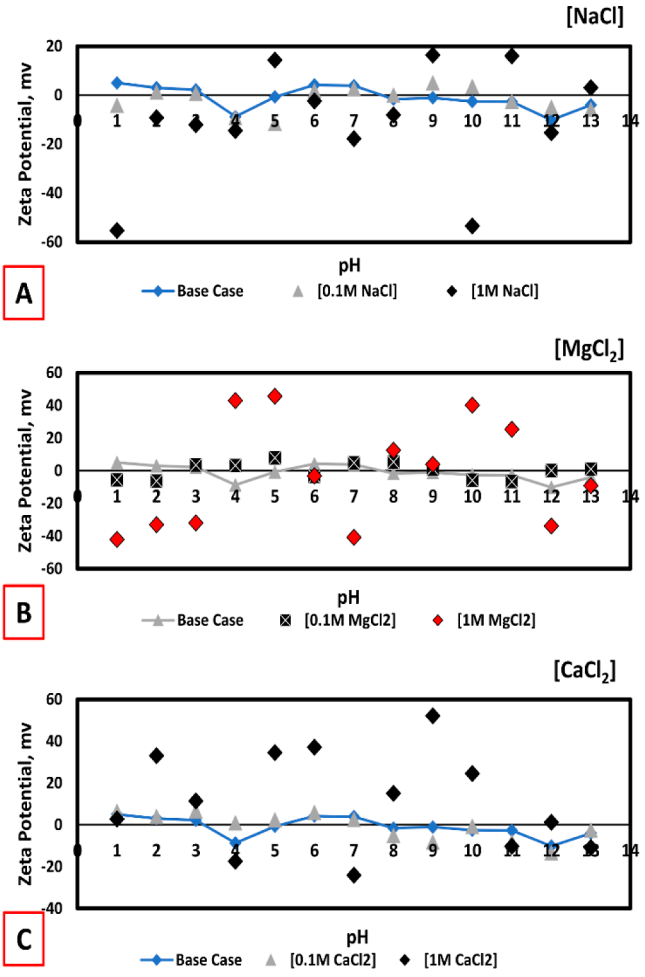

Figure 18. ZP of calcite in 0.1 and 1 M salt solutions. (A) NaCl effect, (B) $MgCl_2$ effect, and (C) $CaCl_2$ effect.

increases the precipitation of ferric ions in the pH environment from 1 to 9. In contrast, 0.1 M $MgCl_2$ turned the calcite surface charge into a negatively charged and more stable system.

Figure 20A shows that the existence of more concentration of Mg^{2+} cations (1 M $MgCl_2$) in the system did not alter the precipitation of ferric ions on calcite minerals, as almost for the whole range of pH environments, the net ZP charge of calcite mineral ranges between −5 and 5 mV. Figure 20C reveals that at a high Fe^{3+} concentration, the calcite surface charge is not affected by 0.1 M $MgCl_2$, except for high pH environments (pH 10−13), where 0.1 M $MgCl_2$ increases the system's stability. Figure 20D corresponds to the effect of 1 M $MgCl_2$ on precipitation of 10,000 ppm Fe^{3+}. Unlike 0.1 M $MgCl_2$, with an increase in the concentration of $MgCl_2$ in the system, calcite minerals show higher stability in near-neutral pH regions. Additionally, it is worth mentioning that the behavior of the system in highly alkaline regions replicates the same trend as a low $MgCl_2$ concentration but with a higher magnitude of a negatively charged system.

The impact of 0.1 M $CaCl_2$ on precipitation of 1500 ppm Fe^{3+} on calcite minerals is depicted in Figure 21A,B. The results indicate that 0.1 M $CaCl_2$ has no significant contribution to iron(III) precipitation on calcite minerals with comparably lower concentrations. However, 1 M $CaCl_2$ affects the stability of the system (Figure 21B) by relatively increasing the ZP charge in acidic environments and pH environments between 7 and 9. In the case of a higher Fe(III) concentration, 0.1 M $CaCl_2$ (Figure 21C) notably affects ferric precipitation in an acidic environment and is reflected in ZP values.

Similarly, 1 M $CaCl_2$ (Figure 21D) influenced the system with the increase of ZP values in low pH environments and also in near-neutral pH environments. Ferric ions are not prone to precipitate by incorporating a higher amount of $CaCl_2$ into the system. Results demonstrate that $CaCl_2$ with high concentration might form better stability and positively impacts ferric ions precipitation in low pH and near-neutral pH environments.

CONCLUSIONS

This work provides a new methodology for incorporating the coreflooding system that is capable of representing downhole squeeze inhibitor treatments in the petroleum industry. The main objective of the developed methodology is to study the dynamic adsorption of chelating agents targeted to inhibit iron sulfide scale formation. The conducted coreflooding tests revealed that various concentrations of aminocarboxylic acids have different adsorption capabilities determined through ferric chelation. The adsorption is also affected by several parameters, such as soaking and the presence of salts. ZP measurements along with the adsorption experiments were performed to investigate the precipitation of iron crystals in calcite minerals. Based on the findings of the work, the following conclusions were made:

1. The optimum chelating agent concentration at 25 °C (77 °F) to inhibit ferric ions was 20 wt %.
2. Low concentrations of divalent cations reduced the adsorption of EDTA by almost 30% at 25 °C (77 °F).
3. The soaking time for EDTA did not result in significant adsorption of EDTA at an ambient temperature. Therefore, the effect of 1 and 2 h of soaking time on EDTA adsorption was not profound.
4. Ferric precipitation is an inevitable phenomenon regardless of the ferric concentration (higher concentrations trigger a bit more precipitation) on calcite minerals, starting from pH environment 1 up to 13.
5. On the other hand, ferrous ions showed erratic trends in acidic pH environments and produced a more stable system. Ferrous ions' considerable instability begins from a neutral pH environment toward the highly alkaline regions at high ferrous concentrations. In contrast, low iron(II) concentrations did not lead to substantial precipitation on calcite minerals.
6. 0.1 M NaCl almost did not affect iron(III) precipitation. At the same time, 1 M NaCl impacted ferric precipitation at relatively low concentrations of Fe^{3+}. In contrast, both 0.1 M NaCl and 1 M NaCl promoted changes in surface charge development by creating negative charge dominant (0.1 M NaCl), positive charge dominant (1 M NaCl), and a relatively stable system at high concentrations of Fe^{3+}.
7. $MgCl_2$ influenced the charge development of calcite and ferric precipitation in high pH environments.
8. $CaCl_2$ with high concentration forms better stability and affects iron(III) precipitation in low pH and near-neutral pH environments.

https://doi.org/10.1021/acsomega.2c01568
ACS Omega 2022, 7, 26137−26153

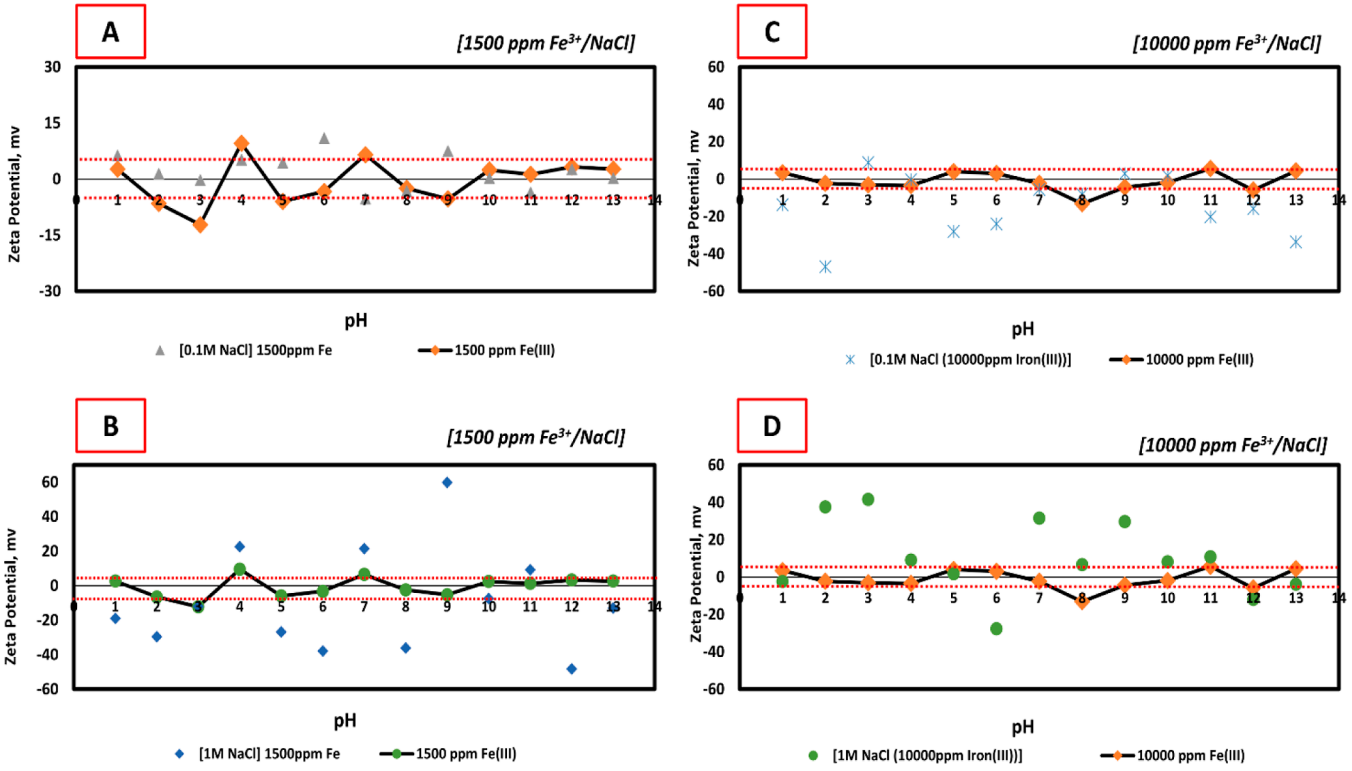

Figure 19. Effect of NaCl on Fe^{3+} precipitation. (A) Low Fe(III) and NaCl concentration, (B) low Fe(III) and high NaCl concentration, (C) high Fe(III) and low NaCl concentration, and (D) high Fe(III) and NaCl concentration.

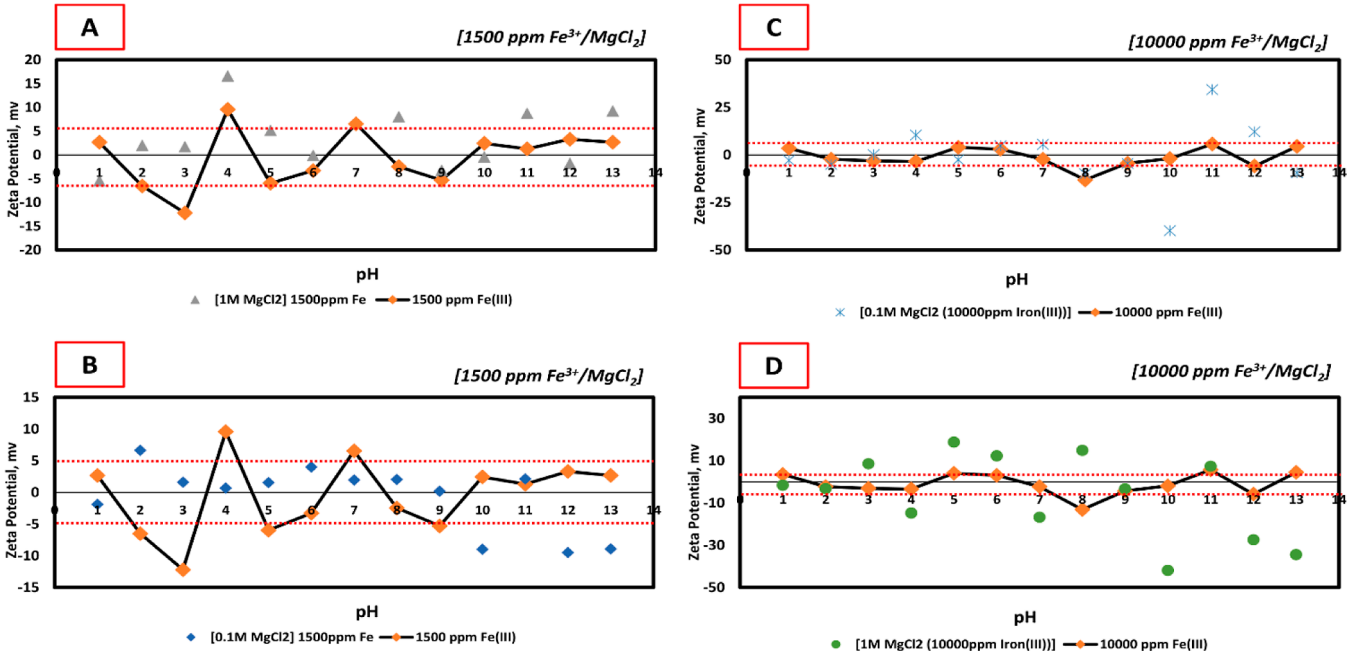

Figure 20. Effect of $MgCl_2$ on Fe^{3+} precipitation. (A) High $MgCl_2$ and low Fe(III) concentration, (B) low Fe(III) and $MgCl_2$ concentration, (C) low $MgCl_2$ and high Fe(III) concentration, and (D) high Fe(III) and $MgCl_2$ concentration.

AUTHOR INFORMATION

Corresponding Authors

Mohamed Mahmoud − *King Fahd University of Petroleum and Minerals, Dhahran 31261, Saudi Arabia;* orcid.org/0000-0002-4395-9567; Email: mmahmoud@kfupm.edu.sa

Muhammad Shahzad Kamal − *King Fahd University of Petroleum and Minerals, Dhahran 31261, Saudi Arabia;* orcid.org/0000-0003-2359-836X; Email: shahzadmalik@kfupm.edu.sa

Authors

Nijat Gasimli − *King Fahd University of Petroleum and Minerals, Dhahran 31261, Saudi Arabia*

https://doi.org/10.1021/acsomega.2c01568
ACS Omega 2022, 7, 26137−26153

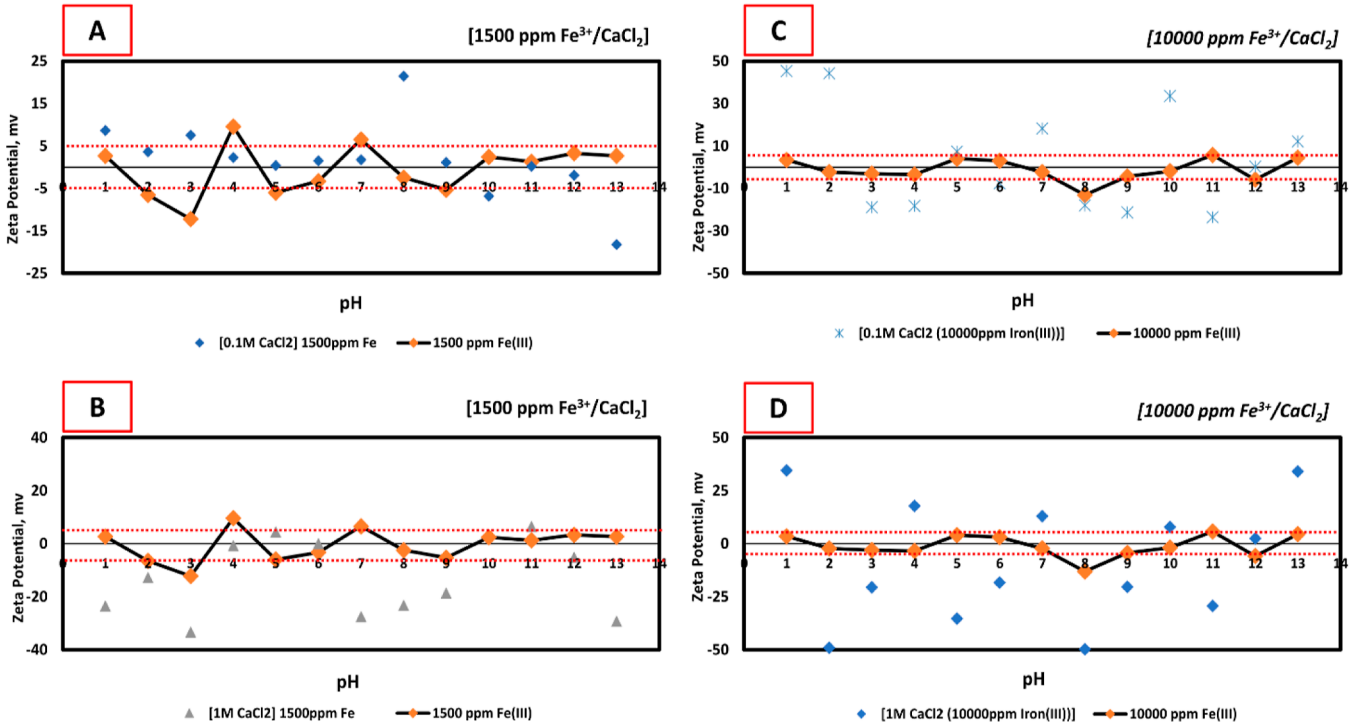

Figure 21. Effect of $CaCl_2$ on Fe^{3+} precipitation. (A) Low Fe(III) and $CaCl_2$ concentration, (B) low Fe(III) and high $CaCl_2$ concentration, (C) high Fe(III) and low $CaCl_2$ concentration, and (D) high Fe(III) and $CaCl_2$ concentration.

Shirish Patil − *King Fahd University of Petroleum and Minerals, Dhahran 31261, Saudi Arabia;* orcid.org/0000-0002-0131-4912

Hamad A. Alsaiari − *Saudi Aramco, Dhahran 31311, Saudi Arabia*

Ibnelwaleed A. Hussein − *Qatar University, Doha 2713, Qatar;* orcid.org/0000-0002-6672-8649

Complete contact information is available at: https://pubs.acs.org/10.1021/acsomega.2c01568

Notes

The authors declare no competing financial interest.

■ ACKNOWLEDGMENTS

The authors acknowledge the College of Petroleum Engineering and Geosciences at the King Fahd University of Petroleum and Minerals for providing laboratory facilities and financial support for conducting this research.

■ REFERENCES

(1) Kamal, M. S.; Hussein, I.; Mahmoud, M.; Sultan, A. S.; Saad, M. A. S. Oilfield Scale Formation and Chemical Removal: A Review. *J. Pet. Sci. Eng.* **2018**, *171*, 127−139.

(2) Olajire, A. A. A Review of Oilfield Scale Management Technology for Oil and Gas Production. *J. Pet. Sci. Eng.* **2015**, *135*, 723−737.

(3) Kelland, M. A. *Production Chemicals for the Oil and Gas Industry*; CRC Press, 2014.

(4) Chen, T.; Wang, Q.; Chang, F. F.; Al-janabi, Y. T. *Corrosion 2016*. Paper No. 7264. 2016, No. 7264; pp 1−14.

(5) Kano, N.; Zhang, S. Adsorption of Heavy Metals on Layered Double Hydroxides (LDHs) Intercalated with Chelating Agents. *Advanced Sorption Process Applications* 2019; pp 1−19.

(6) Ramanathan, R.; Nasr-El-Din, H. Evaluation of Chelating Agents for Iron Sulfide FeS Scale Removal. *Society of Petroleum Engineers—Abu Dhabi International Petroleum Exhibition and Conference 2019*. ADIP 2019, 2019.10.2118/197891-ms.

(7) Bhandari, N.; Kan, A. T.; Ruan, G. G.; Liu, Y.; Zhang, F.; Yan, F.; Alsaiari, H. A.; Zhang, Z.; Dai, Z.; Lu, Y.; Deng, G.; Tomson, M. B. Iron Sulfide Scale Control: A Novel Chemical for Growth Inhibition and Dispersion. *SPE International Oilfield Scale Conference and Exhibition*, 2016. 10.2118/179872-ms.

(8) Al-Harbi, B. G.; Graham, A. J.; Sorbie, K. S. Iron Sulphide Inhibition and Interaction with Zinc and Lead Sulphide. *SPE International Oilfield Scale Conference and Exhibition*, 2018 2018, No. June; pp 20−21.10.2118/190743-ms.

(9) Almubarak, T.; Ng, J. H.; Nasr-El-Din, H. Chelating Agents in Productivity Enhancement: A Review. *SPE Oklahoma City Oil and Gas Symposium* 2017, 2017, No. March; pp 88−112.10.2118/185097-ms.

(10) Hassan, A.; Mahmoud, M.; Bageri, B. S.; Aljawad, M. S.; Kamal, M. S.; Barri, A. A.; Hussein, I. A. Applications of Chelating Agents in the Upstream Oil and Gas Industry: A Review. *Energy Fuel.* **2020**, *34*, 15593.

(11) Tariq, Z.; Hassan, A.; Al-Abdrabalnabi, R.; Aljawad, M. S.; Mahmoud, M. Comparative Study of Fracture Conductivity in Various Carbonate Rocks Treated with GLDA Chelating Agent and HCl Acid. *Energy Fuel.* **2021**, *35*, 19641.

(12) Mahmoud, M.; Elkatatny, S.; Shawabkeh, R.; Bahgat, M. Less Corrosive, Non-Damaging Iron Sulfide Scale Remover. *Abu Dhabi International Petroleum Exhibition & Conference* 2016, 2016, 2016-Janua. 10.2118/183457-ms.

(13) Mahmoud, M. A.; Kamal, M.; Bageri, B. S.; Hussein, I. Removal of Pyrite and Different Types of Iron Sulfide Scales in Oil and Gas Wells without H2S Generation. *International Petroleum Technology Conference* 2015, 2015, 2015-Janua. 10.2523/iptc-18279-ms.

(14) Almubarak, T.; Ng, J. H.; Nasr-El-Din, H. Oilfield Scale Removal by Chelating Agents: An Aminopolycarboxylic Acids Review. *SPE West. Reg. Meet. Proc.* **2017**, *2017*, 1053−1065.

(15) Sorbie, K. S.; Gdanski, R. D. *A Complete Theory of Scale Inhibitor Transport, Adsorption/Desorption and Precipitation in Squeeze Treatments*, 2005. 10.2118/95088-ms.

(16) Kan, A. T.; Dai, Z.; Tomson, M. B. The State of the Art in Scale Inhibitor Squeeze Treatment. *Pet. Sci.* **2020**, *17*, 1579−1601.
(17) Tomson, M. B.; Kan, A. T.; Fu, G. Control of Inhibitor Squeeze via Mechanistic Understanding of Inhibitor Chemistry. *Proceedings—SPE Sixth International Symposium on Oilfield Scale; Exploring the Boundaries of Scale Control*, 2004. 10.2118/87450-ms.
(18) Patroni Zavala, J. A.; Mackay, E. J.; Vazquez, O.; Boak, L. S.; Singleton, M.; Ross, G. The Cost and Value of Field, Laboratory, and Simulation Data for Validating Scale Inhibitor Treatment Models. *SPE International Oilfield Scale Conference*, 2008, No. May 2016, pp 473−493.10.2118/114106-MS.
(19) Halvorsen, E. N.; Marie, A.; Halvorsen, K.; Reiersølmoen, K.; Andersen, T. R.; Biørnstad, C. *New Method for Scale Inhibitor Testing*, 2009; pp 1−11.
(20) Graham, G. M., Collins, I. R., Stalker, R., Littlehales, I. J. *The Importance of Appropriate Laboratory Procedures for the Determination of Scale Inhibitor Performance*. 2002; pp 1−14.10.2118/74679-ms.
(21) Wang, Q.; Al-Nasser, W.; Chen, T.; Liang, F. Calcium Carbonate Scale Inhibition: Effects of EOR Chemicals. *NACE—International Corrosion Conference Series*, 2018, 2018-April (10546); pp 1−12.
(22) Bhandari, N.; Bhandari, M.; Littlehales, I.; Fidoe, J. Development of a Novel Iron Sulfide Scale Inhibitor for Onshore US Application. *SPE International Conference on Oilfield Chemistry*, 2019, 2019.10.2118/193599-ms.
(23) Sutherland, L.; Johnston, C.; Taylor, W. *SPE 164070 The Influence of Turbulence (or Hydrodynamic Effects) on Barium Sulphate Scale Formation and Inhibitor Performance*. 2013; pp 1−9.
(24) Kan, A. T.; Fu, G.; Tomson, M. B. Adsorption and Precipitation of an Aminoalkylphosphonate onto Calcite. *J. Colloid Interface Sci.* **2005**, *281*, 275.
(25) Kan, A.; Yan, L.; Bedient, P. B.; Oddo, J. E.; Tomson, M. B. *Sorption and Fate of Phosphonate Scale Inhibitors in the Sandstone Reservoir: Studied by Laboratory Apparatus with Core Material*, 1991. 10.2523/21714-ms.
(26) Jordan, M. M.; Sjursaeter, K.; Collins, I. Scale Control within North Sea Chalk/Limestone Reservoirs. The Challenge of Understanding and Optimising Chemical Placement Methods and Retention Mechanism: Laboratory to Field. *SPE Prod & Fac* **2004**, *20*, 262 NACE Meet. Pap..
(27) Sulastri, B. N.; Apriyani, S.; Zu'amah, H.; Ardiwinata, A. N.; Purbalisa, W. Adsorption Capacity of Chelating Agent to Adsorb Lead and Arsenic. *IOP Conf. Ser.: Earth Environ. Sci.* **2021**, *648*, 012210.
(28) Kong, S.; Huang, X.; Li, K.; Song, X. Adsorption/Desorption Isotherms of CH4 and C2H6 on Typical Shale Samples. *Fuel* **2019**, *255*, 115632.
(29) Liu, Y.; Hou, J.; Wang, C. Absolute Adsorption of CH4 on Shale with the Simplified Local-Density Theory. *SPE J.* **2020**, *25*, 212−225.
(30) Mohammed, I.; Al Shehri, D. A.; Mahmoud, M.; Kamal, M. S.; Alade, O. Surface Charge Investigation of Reservoir Rock Minerals. *Energy Fuel.* **2021**, *35*, 6003−6021.
(31) Mohammed, I.; Al Shehri, D.; Mahmoud, M.; Kamal, M. S.; Alade, O. S. Impact of Iron Minerals in Promoting Wettability Alterations in Reservoir Formations. *ACS Omega* **2021**, *6*, 4022−4033.
(32) Horikawa, Y.; Murray, R. S.; Quirk, J. P. The Effect of Electrolyte Concentration on the Zeta Potentials of Homoionic Montmorillonite and Illite. *Colloids Surf.* **1988**, *32*, 181.
(33) Mahmoud, M. New Formulation for Sandstone Acidizing That Eliminates Sand Production Problems in Oil and Gas Sandstone Reservoirs. *J. Energy Resour. Technol.* **2017**, *139*, 042902.
(34) Frenier, W. W. Solvent for Removing Iron Oxide Deposits. U.S. Patent 4,623,399 A, 1986; Vol *19*, pp 3−7.
(35) Fredd, C. N.; Fogler, H. S. Alternative Stimulation Fluids and Their Impact on Carbonate Acidizing. *SPE J.* **1998**, *3*, 34.
(36) Al Mahrouqi, D.; Vinogradov, J.; Jackson, M. D. Zeta Potential of Artificial and Natural Calcite in Aqueous Solution. *Adv. Colloid Interface Sci.* **2017**, *240*, 60.
(37) Zaeri, M. R.; Hashemi, R.; Shahverdi, H.; Sadeghi, M. Enhanced Oil Recovery from Carbonate Reservoirs by Spontaneous Imbibition of Low Salinity Water. *Pet. Sci.* **2018**, *15*, 564.
(38) Mohammed, I.; Al Shehri, D.; Mahmoud, M.; Kamal, M. S.; Alade, O. S. A Surface Charge Approach to Investigating the Influence of Oil Contacting Clay Minerals on Wettability Alteration. *ACS Omega* **2021**, *6*, 12841−12852.
(39) Gray, F.; Anabaraonye, B.; Shah, S.; Boek, E.; Crawshaw, J. Chemical Mechanisms of Dissolution of Calcite by HCl in Porous Media: Simulations and Experiment. *Adv. Water Resour.* **2018**, *121*, 369−387.
(40) Heberling, F.; Trainor, T. P.; Lützenkirchen, J.; Eng, P.; Denecke, M. A.; Bosbach, D. Structure and Reactivity of the Calcite−Water Interface. *J. Colloid Interface Sci.* **2011**, *354*, 843−857.
(41) Rady, A.; Nasr-El-Din, H. A. Iron Precipitation in Calcite, Dolomite and Sandstone Cores. *SPE Russian Petroleum Technology Conference*, 2015.10.2118/176574-ms.
(42) Taylor, K. C.; Nasr-El-Din, H. A.; Al-Alawi, M. J. Systematic Study of Iron Control Chemicals Used during Well Stimulation. *SPE J.* **1999**, *4*, 19−24.
(43) Jackson, M. D.; Al-Mahrouqi, D.; Vinogradov, J. Zeta Potential in Oil-Water-Carbonate Systems and Its Impact on Oil Recovery during Controlled Salinity Water-Flooding. *Sci. Rep.* **2016**, *6*, 37363.
(44) Rao, R.; Leja, J. *Surface Chemistry of Froth Rotation Volume 1:Fundamentals*; Springer Sci. Media, LLC, 2004.
(45) Nande, S. Application of Machine Learning for Closure Pressure Determination. *SPE Annual Technical Conference and Exhibition*, 2018, 2018-Septe(September); pp 24−26.10.2118/194042-stu.

https://doi.org/10.1021/acsomega.2c01568
ACS Omega 2022, 7, 26137−26153